2024 Scienceline Publication

Journal of Civil Engineering and Urbanism

Volume 14, Issue 2: 30-62; June 25, 2024 **ISSN-2252-0430**

DOI: https://dx.doi.org/10.54203/jceu.2024.4

Investigation of the Engineering Properties of Glass Fiber Reinforced Concrete (GRC) Cured with Internal Resistance

Sıtkı Koc[1], Serkan Subasi[2], Muhammed Marasli[3], and Volkan Ozdal[3]

[1]*Master's Student, Duzce University, Postgraduate Education Institute, Civil Engineering Department, Duzce, Turkiye*
[2]*PhD, Prof. Dr., Duzce University, Engineering Faculty, Civil Engineering Department, Duzce, Turkiye*
[3]*Fibrobeton Company, R&D Center, Duzce, Turkiye*

Corresponding author's Email: sitkikoc@outlook.com

RESEARCH ARTICLE

PII: S225204302400004-14

Received: January 14, 2024

Revised: May 28, 2024

Accepted: June 03, 2024

ABSTRACT

In this study, it was aimed to produce glass fiber reinforced concrete (GRC) samples cured with internal resistance by placing resistance wires at different distances within the concrete molds and applying electric current at various voltages, while the mold surfaces were covered with stretch film. The engineering properties of these samples were then investigated. Previous studies have shown that the mechanical properties of conventional concrete, which were subjected to different curing methods, improved compared to samples that did not undergo any curing process. This study aimed to enhance both the engineering properties of the concrete samples and to accelerate the curing process. Glass fiber reinforced concrete (GRC) with dimensions of 50×50×4 cm was produced, and 25, 35, and 45V resistances were applied to three different molds with wire spacing of 5cm, 6cm, and 7cm. With this application, the GRC samples were subjected to internal resistance curing for the first 24 hours. By applying three different voltages to molds with three different wire spacings, 9 concrete samples were produced, along with 1 reference sample that did not contain any resistance wires and was not subjected to any curing process, making a total of 10 different concrete samples. After curing, the concrete samples were cut into 16cm×4cm×4cm GRC mechanical test specimens. The obtained specimens were tested for 7, 14, and 28 day compressive strength, flexural strength, unit weight, and ultrasonic pulse velocity. To examine the microstructure of the GRC samples, Scanning Electron Microscopy (SEM), Thermogravimetric Analysis (TGA), and Fourier Transform Infrared Spectroscopy (FT-IR) analyses were conducted. These analyses investigated the physical and chemical development processes of the samples, mass losses, products formed after hydration, and structural behaviors. As a result, it was observed that the early-age strength properties of GRC samples cured with internal resistance showed a partial increase compared to the reference sample that was not internally cured, especially in the 7-day samples. In the 14 and 28-day strength comparisons, it was observed that the cured samples showed improvement in flexural strength. According to the data obtained, the samples subjected to 35 volts of electric current yielded better results, especially in the early ages, compared to the reference sample.

Keywords: Glass Fiber Reinforced Concrete (GRC), Internal Resistance Curing, Microstructure, Engineering Properties

INTRODUCTION

From past to present, one of the most essential needs of humanity has been shelter. Early humans met their initial shelter needs in caves they constructed. In the evolving and changing world, especially in the years following the Industrial Revolution, the advancement of technology has led to the construction of buildings with high comfort and quality tailored to meet various needs. In this context, the rapid development of technology, the improvement of laboratory conditions, and the intensive efforts of researchers have prompted the construction industry to seek different methods to increase production speed and produce higher quality materials. Particularly, increasing the production speed of prefabricated or factory-made concrete structural elements has become crucial to meet high demand. For this reason, the reduction of concrete curing times and the improvement of material properties have become focal points of research.

The strength and durability characteristics of concrete generally vary depending on where it is used. Today, especially in reinforced concrete systems (such as shear walls, beams, and columns), concrete is commonly used in combination with steel reinforcement. Additionally, the introduction of fibers in the production of precast concrete elements, aimed at enhancing material properties, has become particularly important. These fibers, which are homogeneously distributed within the concrete elements, significantly contribute to the composite structure both

during and after setting. These emerging composite materials have become a focal point for architects and engineers due to their design versatility, high-performance strength, and wide range of application compared to traditional concrete. They have also gained importance as a subject of research. Moreover, another significant research area has been the increase in the production speed of these composite materials (Maraşlı M., 2019).

To shorten curing times and achieve early setting of concrete, various curing methods have been developed. Research has aimed not only to reduce curing times but also to enhance the mechanical and durability properties of concrete elements. Achieving high strengths at early ages and making concrete rapidly usable are of great importance in this context. Therefore, researchers have developed numerous improvement methods, allowing for the attainment of desired mechanical and durability properties in short periods (Backe et al., 2001). These methods generally include electrical curing, steam curing, microwave curing, hot water curing, autogenous curing, and modifications to hot water curing methods (Kjellsen, 1996).

The applicability of electrical energy or electrical resistance in determining the setting time of concrete samples has been demonstrated through research. It has been shown that using electrical energy to raise the internal temperature of fresh concrete can accelerate the hydration process, and the potential effects of this method have been investigated (Backe et al., 2001; ,Whittington et al. 2015).

In regions with cold climates, snow, ice, and frost events significantly disrupt the normal flow of life. Although not widely used, research has shown that heating with electrical resistance can mitigate these adverse effects (Canbaz et al., 2018).

In precast concrete elements, thermal curing is generally quite useful. Raising the temperature of the concrete to higher levels compared to traditional methods enhances the hydration process of the cement and enables the concrete to gain strength in much shorter periods (Lothenbach et al., 2007). In such cases, the thermal curing process is influenced not only by the determining parameters of the applied method but also by the minerals and additives present in the concrete (Pavlenko, 1994).

There are few studies that observe the potential effects of embedding electrical resistance wires into fresh concrete and covering the mold surfaces with airtight stretch film to prevent moisture loss. In this context, embedding electrical resistance within concrete to increase the internal temperature and produce hydration products more quickly and with higher quality compared to traditional methods is of significant importance. In the study of internal resistance curing of concrete, the goals were to increase production speed, enhance the quality of the produced material, and achieve a healthy product in cold environmental conditions. For this study, concrete molds with dimensions of 50cmx50cmx4cm were specially produced, and resistance wires were inserted with spacings of 5cm, 6cm, and 7cm. The internal resistance curing method involved applying voltages of 25V, 35V, and 45V to these wires, and the mold surfaces were covered with stretch film to prevent moisture loss. To compare the samples produced with the electrical curing method, a reference concrete sample with no applied voltage and an open surface was also produced. The internal temperatures, surface temperatures, mechanical properties, and microstructural characteristics of all these samples were investigated.

Early detection of the strength of concrete material is crucial for determining both the performance and economic quality and safety level of the structure. To achieve early strength determination, many methods have been developed to accelerate concrete curing (Topçu et al., 2008; Deniz, 2011).

In a study conducted by Rahmun T. Nazmul et al., the aim was to explore the potential application of hydrophilic hemp fibers as an alternative to existing chemical products used in concrete for internal curing. The study found that the highest relative humidity (>93%) was achieved when using smaller-sized (<2.36mm) hemp fibers compared to other fiber samples. This research revealed that even small-sized hemp fibers can serve as a natural internal curing additive when used within concrete (Nazmul *et al.*, 2023).

El-Dieb et al. (2015) conducted a study to investigate the effects of adding water-soluble polymers, Polyethylene Glycol (PEG) and Polyacrylamide (PAM), to curing water for concrete. The study aimed to examine the properties of Portland cement, including water retention, degree of hydration, water absorption, pore permeability, and microstructural characteristics, by replacing cement with silica fume and without using silica fume. The mixtures containing PEG and PAM were found to exhibit better water retention, higher non-evaporative water content, lower water absorption, and reduced permeability compared to polymer-free mixtures. The microstructural analysis revealed that self-curing mixtures, including those with added polymers and with or without silica fume, had a denser microstructure and fewer micro-cracks compared to similar non-cured mixtures (El-Dieb et al. 2015).

Nie et al. (2018) conducted a study on thermal curing of concrete, suggesting that it creates large pores within the concrete, which significantly reduces its durability. They investigated the effects of using saturated lightweight aggregate as a replacement aggregate in concrete mixtures, focusing on the mechanical properties, transport properties, and microscopic characteristics of the mixtures cured internally with heat. The study found that the use of saturated lightweight fine aggregate supports cement hydration, leads to the formation of denser hydration products, and benefits the formation of the interfacial transition zone. Additionally, it was demonstrated that internally heat-cured mixtures exhibited long-term performance similar to or even better than mixtures cured under ambient conditions (Nie et al., 2018).

Yoo et al. (2018) conducted a study to examine the effects of different curing conditions on the free shrinkage behavior of ultra-high performance fiber-reinforced concrete (UHPFRC). In this study, a series of open and closed prismatic UHPFRC samples were produced for drying and autogenous shrinkage measurements. These samples were subjected to heat steam curing (at 90°C) and ambient curing conditions. Two types of embedded strain gauges were installed in the samples. The test results showed that heat curing was effective in improving the mechanical properties, strength, elastic modulus, and fracture energy absorption capacity of UHPFRC samples at an early age. Based on a literature review, the researchers proposed an optimized model and also successfully predicted the autogenous shrinkage development of UHPFRC samples under both ambient and heat curing conditions using an equivalent age method Yoo et al., 2018).

Cong et al. (2016) found that heating an electrically conductive cable embedded in the mixture for curing was highly efficient among different curing methods. In their study, Cong et al. investigated the effects of varying the length, winding type, and electrical resistance application time of the conductive wire on the setting times of concrete. Simulations using a tool called Gen Midas were also conducted to explore potential outcomes in temperature distribution. The experiments showed that the concrete samples reached a constant temperature of 45°C in 16 hours. They found that if the wire length was too long, the temperature would increase too quickly, resulting in inefficient hydration, while if it was too short, the temperature would be too low, also leading to inefficient hydration. They concluded that when all variables were optimized, it was possible to control the temperature of the mixture within the desired timeframe (Cong et al., 2016).

Uygunoğlu and Hocaoğlu (2018) investigated hydration times by applying electrical voltages at different ranges to concrete with varying dosages, using fixed molds. For this experiment, concrete with dosages of 250, 300, 350, and 400 was placed into 10×10×35 cm molds. The concrete samples were then cured by applying electrical currents of 0, 40, 60, 80, and 100 volts for 24 hours. It was observed that when a constant electrical current of 100V was applied to different dosages of concrete, the setting times were reduced compared to the reference sample. Scanning Electron Microscopy (SEM) images of the 300 dosage sample showed that increasing electrical resistance accelerated hydration. They suggested that both increasing the concrete dosage and raising the electrical resistance could shorten the hydration time (Uygunoğlu and Hocaoğlu, 2018).

MATERIAL AND METHODS

Material

In this study, the aim was to shorten the setting time of Concrete Thermal Blocks (CTBs) used as exterior cladding materials and to prevent any decline in mechanical strength of the concrete samples as a result of the thermal processing carried out to achieve this time reduction. The concrete mixtures were placed into MDF (Medium Density Fiberboard) laminated molds specifically produced in dimensions of 50×50×4 cm. Since CTBs are intended for use as exterior materials, MDF laminated molds were used to achieve smoother surface samples. The molds were manufactured with a two-way disassemblable design. The molds were drilled with a 1 mm diameter drill at intervals of 5, 6 and 7 cm, in a single direction on both sides. Electrical conductive wires with a diameter of 0.5 mm were passed through the drilled holes. Three different molds were connected in parallel to each other using conductive wires. The surface of the molds was covered with stretch film to prevent moisture loss from the concrete mixture. A voltage was applied to the mold from a constant power source for 24 hours.

By evaluating the results obtained from this study, it is aimed to contribute to the literature and future research on internal resistance curing methods for concrete samples with different applications.

The devices and materials used in the experiment, aside from the cement paste, are summarized below:

- MDF Laminated Molds (50×50×4 cm in size)
- Electrical Conductive Resistance (0.5 mm diameter)
- Power Supply

• Stretch Film

The chrom-nickel resistances installed in the molds contain 80% nickel and 20% chromium. These resistance wires provide high thermal endurance and corrosion resistance. The concrete samples used in the study were prepared as Premix CTB at Fibrobeton Inc.'s Düzce Factory. Figure 1 shows AR Glass Fiber Reinforcement during the Premix CTB production phase.

Figure 1. Premixed mix preparation

Here is the list of CTB mixture materials and their information:

- **Cement**: CEM II/B-L 42.5R White Portland Limestone Cement
- **Aggregate**: Silica sand suitable for CTB production
- **Mineral**: Metakaolin
- **AR Glass Fiber**: 12mm cut Alkali-Resistant Glass Fiber
- **Acrylic Polymer**: Vinyl acrylic copolymer aqueous solution
- **Superplasticizer**: Polycarboxylate ether-based superplasticizer
- **Water**: Well water collected from the Düzce basin

Cement

In this study, CEM II/B-L 42.5R White Portland Limestone Cement was used in accordance with TS EN 197-1. Due to its significant clinker content, it provides the necessary early and final strength, while its components grant the cement high workability. [36] The cement used in this study was produced by Çimsa Çimento San. A.Ş. The laser particle size distribution analyses shown in Figure 2 were obtained from the Laser Particle Sizer device at Fibrobeton A.Ş. The cements used throughout the experiment were supplied by Fibrobeton A.Ş.

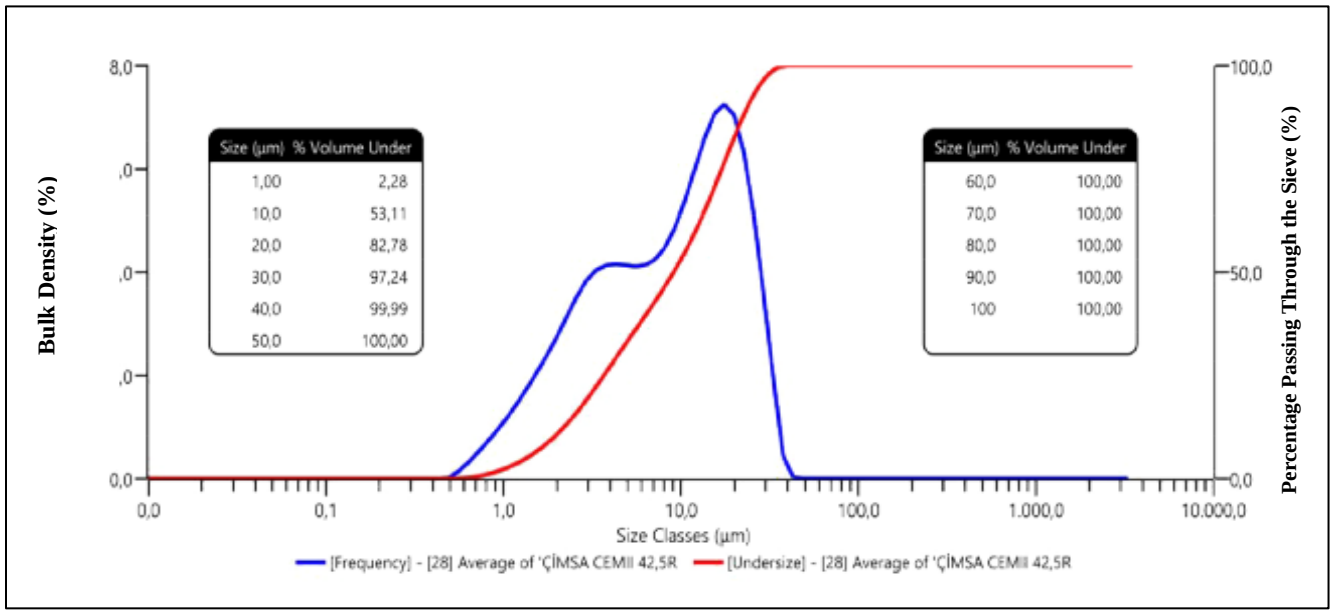

Figure 2. Laser particle size distribution results of the used cement

Water

Water used in concrete production and curing must be clean. Additionally, it should not contain substances such as clay, silt, acid, chlorides, organic matter, sulfate, oil, and industrial waste that could adversely affect the properties of fresh and hardened concrete. In the experiments conducted, well water collected from the Düzce basin was used as the mixing water.

Aggregate

In this study, silica sand used in standard GRC production, which is manufactured by Fibrobeton A.Ş., has been substituted as aggregate. The silica sands used in the mixtures were obtained from Çeliktaş A.Ş. The laser particle size distribution analyses of the aggregates were performed within Fibrobeton A.Ş. The results of the laser particle size distribution analyses are shown in Figure 3.

Metakaolin

Metakaolin is a reactive pozzolan produced by the calcination of the natural clay mineral known as kaolin or kaolinite at high temperatures (approximately 600-800 °C), followed by grinding to reduce the particle size into very fine particles (Yıldırım et al., 2018). The metakaolin used in this study was obtained from Fibrobeton A.Ş. The laser particle size distribution analysis results for the metakaolin are shown in Figure 4.

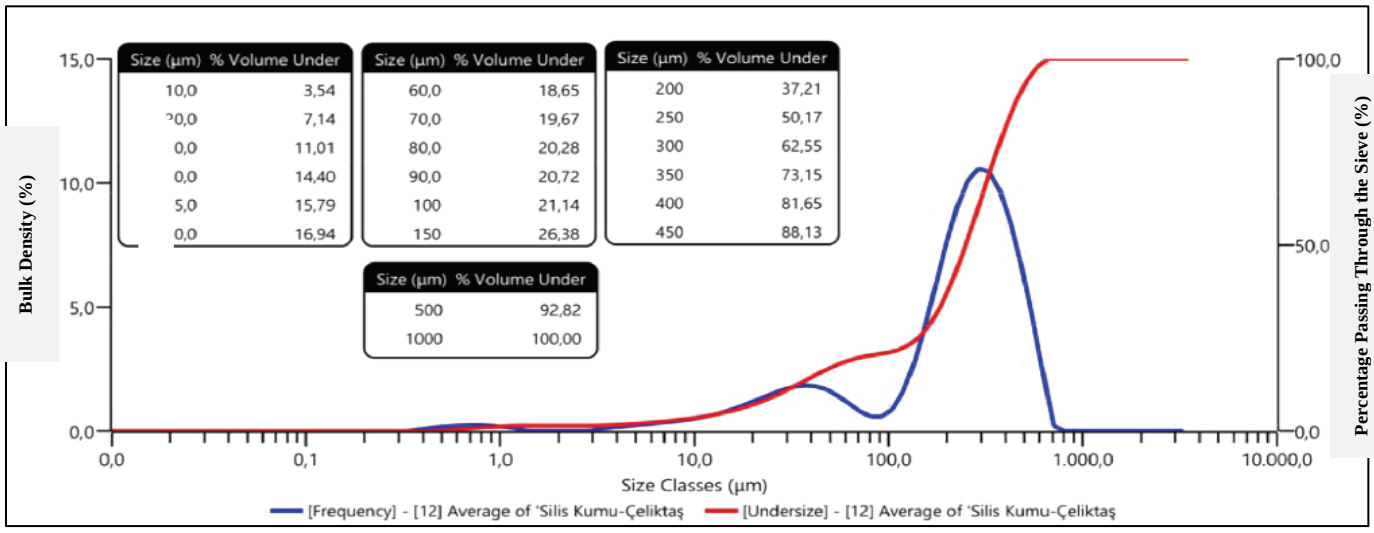

Figure 3. Laser particle size distribution results of the used aggregate

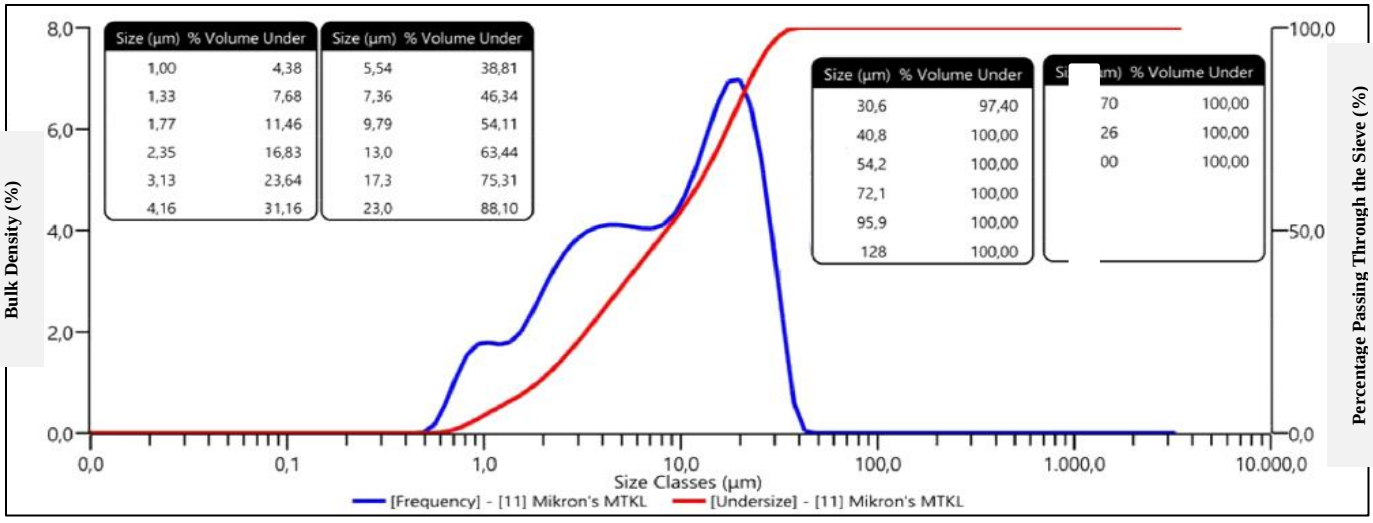

Figure 4. Laser particle size distribution results of the used metakaolin

AR glass fiber

Glass fibers exhibit the characteristic properties of typical glass. They are hard, resistant to corrosion, and react minimally with other materials, similar to conventional glass. The high strength of glass fibers helps minimize defects on the fiber surface and within the concrete samples, and ensures that any defects that do occur are relatively small. These fibers should be cut to ensure a minimum length-to-diameter ratio of 10/1. They can be cut and used according to the desired fiber length (Ali et al., 2019). The AR (alkali-resistant) glass fibers used in this experiment were produced by Nippon. The AR glass fibers for the experiment were supplied by Fibrobeton A.Ş.

Superplasticizer and its properties

Water reducers or superplasticizers are known to be used for various purposes, such as increasing the strength of the produced concrete by reducing the water/cement ratio, improving its workability, facilitating the placement of the concrete mix into the production molds, reducing the cement content in mass concrete to lower the heat of hydration, and enhancing the resistance of concrete to freeze-thaw cycles (Doğan et al., 2022). The polycarboxylate ether-based superplasticizer used in the experiment was obtained from Fibrobeton A.Ş.

Acrylic polymer and its properties

The vinyl acrylic copolymer aqueous solution used in the experiment was obtained from Fibrobeton A.Ş.

Methods

In the study investigating the mechanical properties of CTB concrete cured by the internal resistance method, the work plan consists of 5 steps.

The first step involved the preparation of suitable molds. Three molds, each measuring 50×50×4 cm, were prepared with uniaxial holes drilled at intervals of 5 cm, 6 cm, and 7 cm with a 1 mm diameter. Conductive chrome-nickel alloy wires with a diameter of 0.5 mm were passed through these holes. Before the concrete was poured, these molds were connected in parallel, and different voltages were applied until the wires reached a stable temperature. While the wires were at a stable temperature, measurements of the current passing through the wires and the temperature of the wires were taken. The goal here was to determine the optimal voltage for the experiment by measuring the temperature balance in advance, to achieve the optimal temperature. It was observed that when applying low voltages (20V and below), there was no significant increase in temperature, whereas high voltages resulted in very high temperatures that could negatively affect the sample. Therefore, based on the temperatures obtained in preliminary tests, it was decided to apply voltages of 25V, 35V, and 45V.

In the second step, the standard CTB mix recipe from Fibrobeton A.Ş. was used. The mix was prepared according to the recipe in a Premix production format.

The third step involved placing the concrete mix into the prepared molds and starting the application with internal resistance, followed by examining the thermal changes of the fresh concrete until it hardened. This examination was recorded for 24 hours using a thermal camera. Voltage was applied to the curing samples for 24 hours. Each application was conducted by applying the same voltage to 3 molds (5 cm resistance spacing, 6 cm resistance spacing, 7 cm resistance spacing). In total, 9 molds were subjected to electrical currents of 25V, 35V, and 45V (3 molds for each voltage). Finally, a reference sample with no applied current or curing method was monitored for 24 hours using a thermal camera. All these applications and examinations were recorded, forming the third part of the experimental work plan.

In the fourth step, the hardened concretes were removed from the molds. The produced concrete samples of size 50×50×4 cm were cut into appropriate dimensions (160×40×40 mm) using a concrete saw for mechanical testing. The cube and prismatic test samples were cut from the concrete between the resistance wires. For samples of sizes 160×40×40 mm at 7, 14, and 28 days, unit weight, ultrasonic pulse velocity, flexural strength, and compressive strength tests were conducted.

In the final step, small pieces and powdered products taken from all mechanically tested samples were brought to the Düzce University Scientific and Technological Research Application and Research Center for microstructure analysis. TGA, FT-IR, and SEM analyses were performed on a total of 9 samples from different molds with different voltages and one reference sample.

The naming of the produced samples and the production plan are given in Table 1.

Table 1. Sample production plan table

Concrete code	Resistance distance	Voltage power
CTB-REF	-	-
CTB-5C-25V	5 cm	25 Volt
CTB-6C-25V	6 cm	25 Volt
CTB-7C-25V	7 cm	25 Volt
CTB-5C-35V	5 cm	35 Volt
CTB-6C-35V	6 cm	35 Volt
CTB-7C-35V	7 cm	35 Volt
CTB-5C-45V	5 cm	45 Volt
CTB-6C-45V	6 cm	45 Volt
CTB-7C-45V	7 cm	45 Volt

Preparation of test molds

In the initial phase of the study, the design of the concrete production mold to be used in internal resistance curing method experiments was carried out. After a literature review, four MDF LAM concrete molds with

dimensions of 50×50×4 cm (width, length, height) were produced to obtain the most useful samples with the clearest results from the GRC concrete to be produced. Three of the produced concrete molds were drilled with 1 mm diameter holes at intervals of 5 cm, 6 cm, and 7 cm, with one-sided entry and exit. Electrical conductive resistors with a diameter of 0.50 mm were placed in the entry and exit parts of the three different molds. These molds were connected in parallel with cables to apply the same voltage to them. The schematic representation of the GRC production molds is shown in Figure 5. In Figure 6, molds with electrical conductive wires placed and connected in parallel with conductive cables are shown.

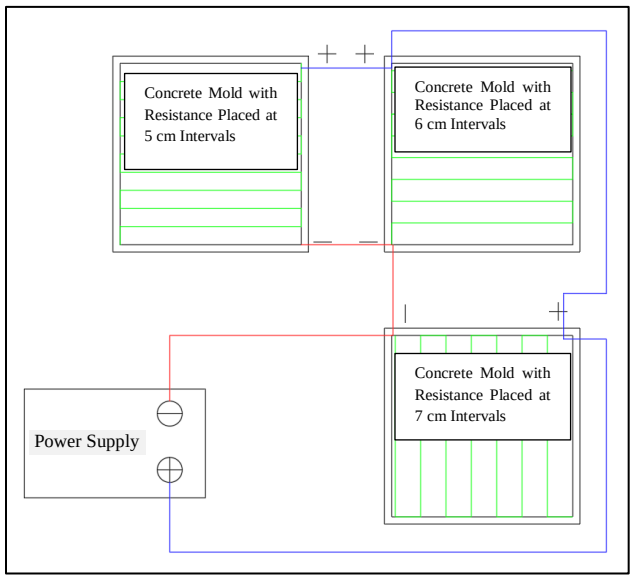

Figure 5. Electrical connection diagram of GRC production molds

Figure 6. Electrical connection diagram of GRC production molds

Preparation of concrete Mix and placement in test molds

In this study, the standard CTB mix produced by Fibrobeton A.Ş was used. The mix was prepared according to the specified recipe using the Premix application method. Before placing the concrete mix, the existing molds were cleaned and oiled. The prepared mix was carefully placed into three molds containing internal resistance wires. This process was repeated four times to produce three samples with different voltages and one reference sample. Except for the reference sample, all other molds were covered with plastic wrap to prevent moisture loss from the concrete. In Figure 7, concrete mixes placed in molds and covered with plastic wrap are shown.

Recording of temperature variation values with a thermal camera

The thermal camera used in this study is the PI400i model from Optiris. With the 80-degree lens on the thermal camera, temperature readings were easily taken over an area of approximately 5 square meters. Test data compliant with standards were preloaded into the system for the molds, which were covered with plastic wrap immediately after the concrete was poured (Maraslı et al., 2023). Once the thermal camera was ready, voltage was applied from the power supply, and tests on the fresh concrete began. The experimental setup with the thermal camera in place is shown in Figure 8.

Determination of the unit weight of hardened concrete

The determination of the unit weight of hardened concrete samples was conducted in accordance with the TS EN 12390-7 standard (Türk Standartları Enstitüsü, 2002). Four samples were produced from each concrete batch, and their dimensions were measured using a caliper. The weights of the concrete samples, which had been cured under room conditions, were recorded, and unit weight values were obtained. The test samples are shown in Figure 9. The unit weight values were calculated according to Equation 2.1.

$$S_k = \frac{w}{v}\,(g/cm3) \qquad (2.1)$$

In this equation;

S_k: Dry unit weight of hardened concrete (g/cm^3)

$W^{:}$ Dry weight of the hardened concrete sample (g)

V: Volume of the hardened concrete sample (cm^3)

Ultrasonic pulse velocity test

The concrete samples were tested using non-destructive methods without subjecting them to destructive testing methods. In this context, the samples were subjected to the Ultrasonic Pulse Velocity test. The test was conducted in accordance with ASTM C 597 standards, using four samples of 40×40×160 mm dimensions from each concrete batch. Measurements were taken on samples at 7, 14, and 28 days. The formula for the Ultrasonic Pulse Velocity test is shown in Equation 2.2.

$$V = \frac{L}{\Delta t} \text{ (km/sn)} \quad (2.2)$$

In this equation;

V = Ultrasonic Pulse Velocity (km/sn)

L = Passing Distance (mm)

Δt = Passing Time (μs)

The application of the Ultrasonic Pulse Velocity test is shown in Figure 2.10.

Figure 7. Concrete mixes placed in molds and covered with plastic wrap.

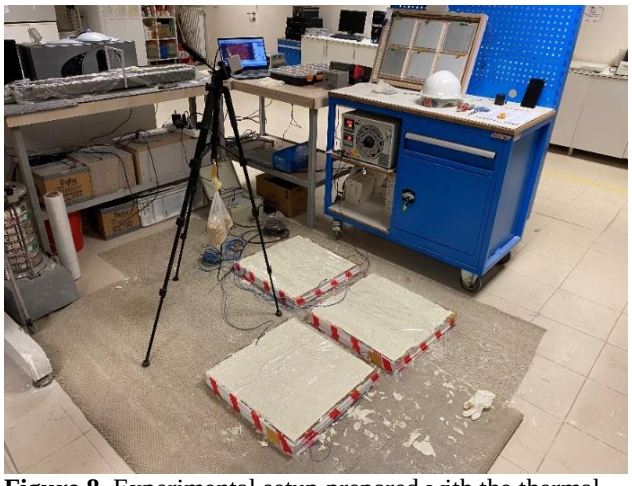

Figure 8. Experimental setup prepared with the thermal camera.

Figure 9. Experimental setup prepared with the thermal camera.

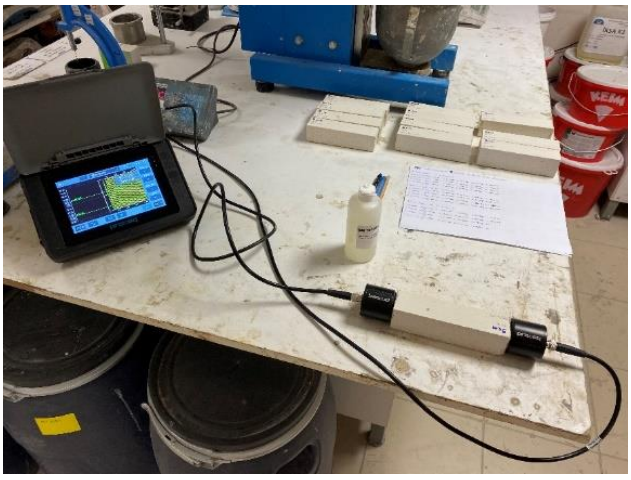

Figure 10. Application of the ultrasonic pulse velocity test.

Flexural strength test

Flexural strength tests were conducted using samples of 40×40×160 mm dimensions obtained from GRC concrete, with four samples from each concrete batch. The

flexural strength tests were performed in accordance with the TS EN 12390-5 standard on samples at 7, 14, and 28 days. The application phase of the flexural strength test is shown in Figure 11.

Figure 11. Flexural strength test setup.

Compressive strength test

Compressive strength tests were conducted in accordance with the TS EN 12390-3 standard on samples at 7, 14, and 28 days. The application phase of the compressive strength test is shown in Figure 12.

Figure 12. Compressive strength test setup.

Microstructure analyses

Microstructure properties are as crucial as the strength values obtained from destructive tests for concrete samples. In this study, TGA, FT-IR, and SEM analyses were performed on the sample groups produced. The test samples prepared for microstructure analysis are shown in Figure 13.

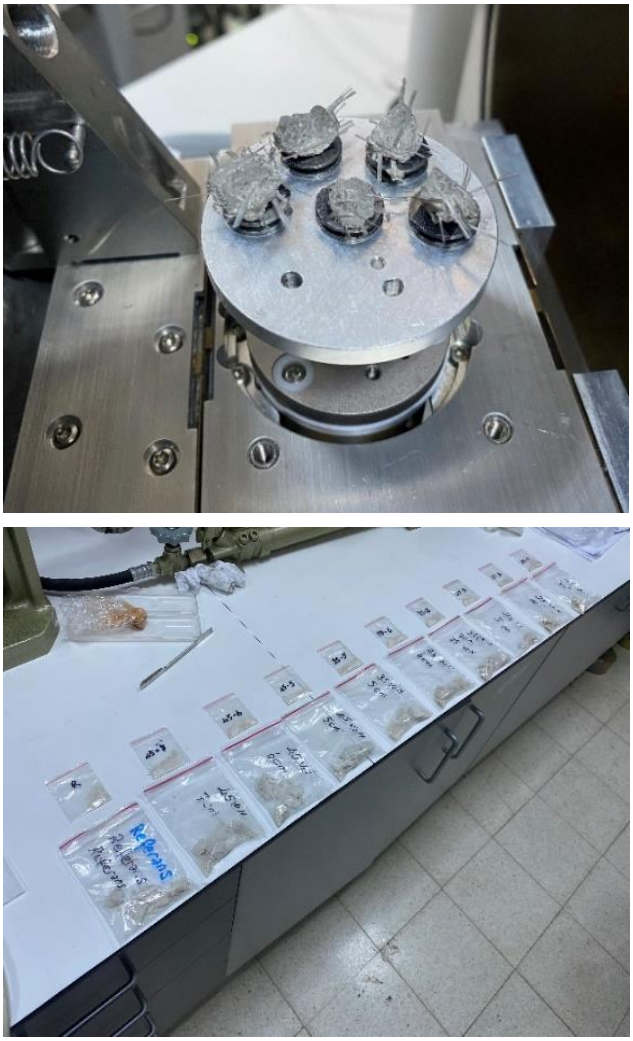

Figure 13. Samples prepared for microstructure analysis.

RESULTS AND DISCUSSION

Unit weight test results

The results of the unit weight test conducted on samples cured using the internal resistance method and the reference sample are shown in Figure 14.

Upon examining the results, it is observed that, except for the CTB-5C-35V and CTB-6C-35V samples, the unit weight of concrete decreases over time. Considering the

data in Figure 14, it is evident that the samples cured with internal resistance have lower unit weight values compared to the reference sample. Among the samples cured with internal resistance, those obtained from concrete subjected to a 25V electrical current exhibited the lowest unit weight values compared to other curing methods. The difference in unit weight between early-age cured samples and the reference sample was significant; however, by day 28, this difference showed a notable reduction. On day 7, the highest unit weight value was observed in the reference sample (1.97 g/cm³) and the lowest in CTB-6C-25V (1.89 g/cm³), with a ratio of 4.2%. By day 28, this ratio decreased to 3.2% between these two samples. Considering all samples, on day 28, CTB-5C-35V exhibited the highest unit weight value, followed by CTB-6C-35V, and then the reference sample. The unit weight of the CTB-5C-35V sample was 1.5% higher compared to the reference sample on day 28. These results indicate that while no linear relationship was established among the samples, the CTB-5C-35V sample provided the highest unit weight value at later ages.

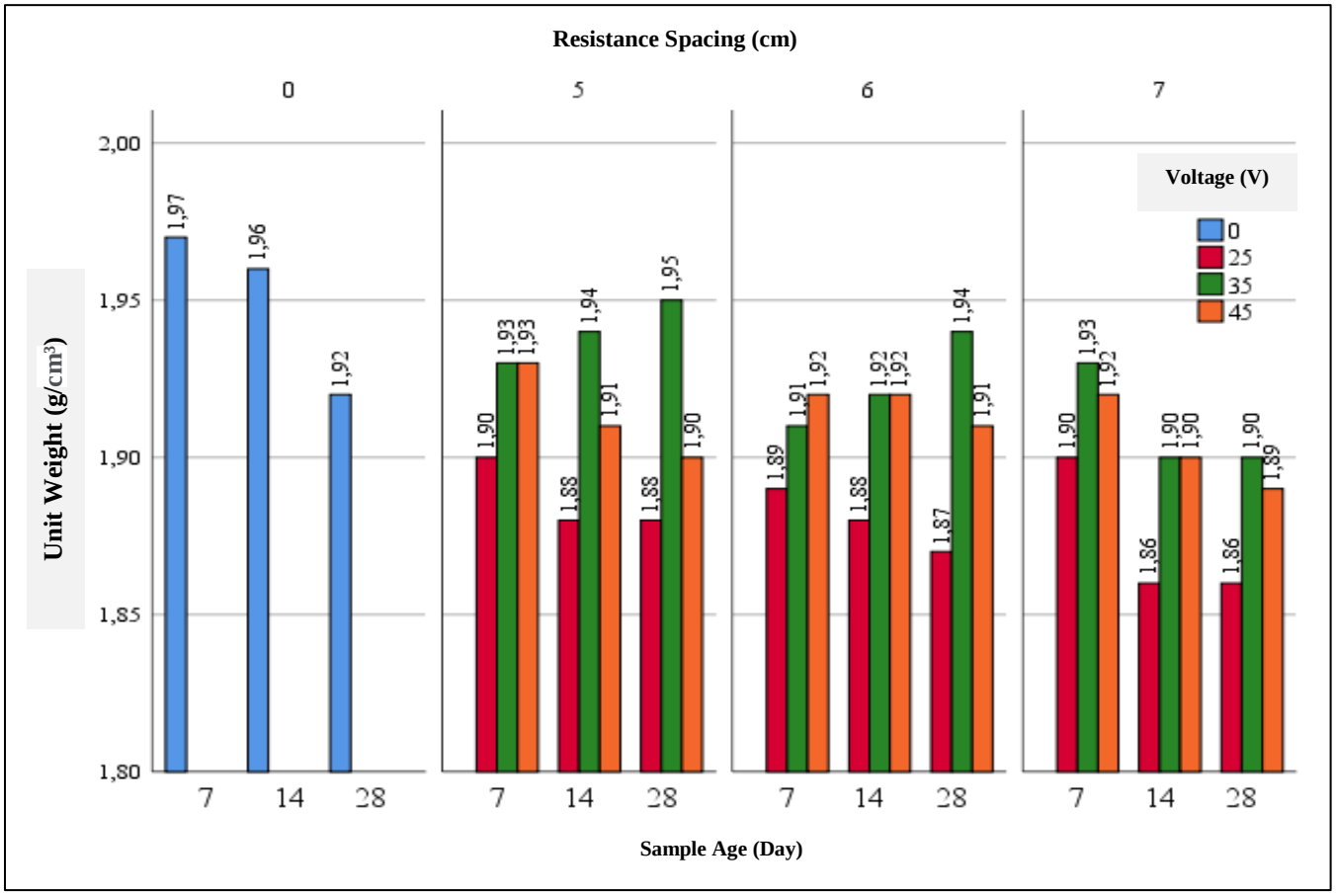

Figure 14. Unit weight test data

Ultrasonic pulse velocity test results

Ultrasonic pulse velocity tests were conducted on all samples, and the test results are shown in Figure 15 Based on these data, it is observed that for early-age samples cured with internal resistance, the ultrasonic pulse velocity decreases with increasing voltage. When comparing early-age reference samples with those cured using internal resistance, it was found that the reference sample had an ultrasonic pulse velocity 4.5% higher than the CTB-7C-45V sample, which exhibited the lowest value at early age. On days 7, 14, and 28, the ultrasonic pulse velocity values of the reference sample were higher compared to those of samples cured with internal resistance. On day 14, the reference sample had the highest value, while the closest values were observed in the CTB-7C-35V and CTB-5C-35V samples, which had ultrasonic pulse velocity values just 1% below the reference sample. By day 28, the ultrasonic pulse velocity of the CTB-5C-35V sample was very close to that of the reference sample, with the difference reduced to 0.5%. These results indicate that

over time, the ultrasonic pulse velocity increases in samples cured with internal resistance, suggesting improved concrete quality. Considering the data, CTB-5C-35V showed the next optimal value after the reference sample. It was observed that curing with 45V resulted in lower ultrasonic pulse velocity values compared to samples cured with 25V and 35V. Overall, no significant decrease in ultrasonic pulse velocity was noted among the samples, indicating good concrete quality. An examination of the results from compressive strength and ultrasonic pulse velocity tests revealed no direct correlation between the two, which can vary depending on the material mix characteristics and conditions within the concrete.

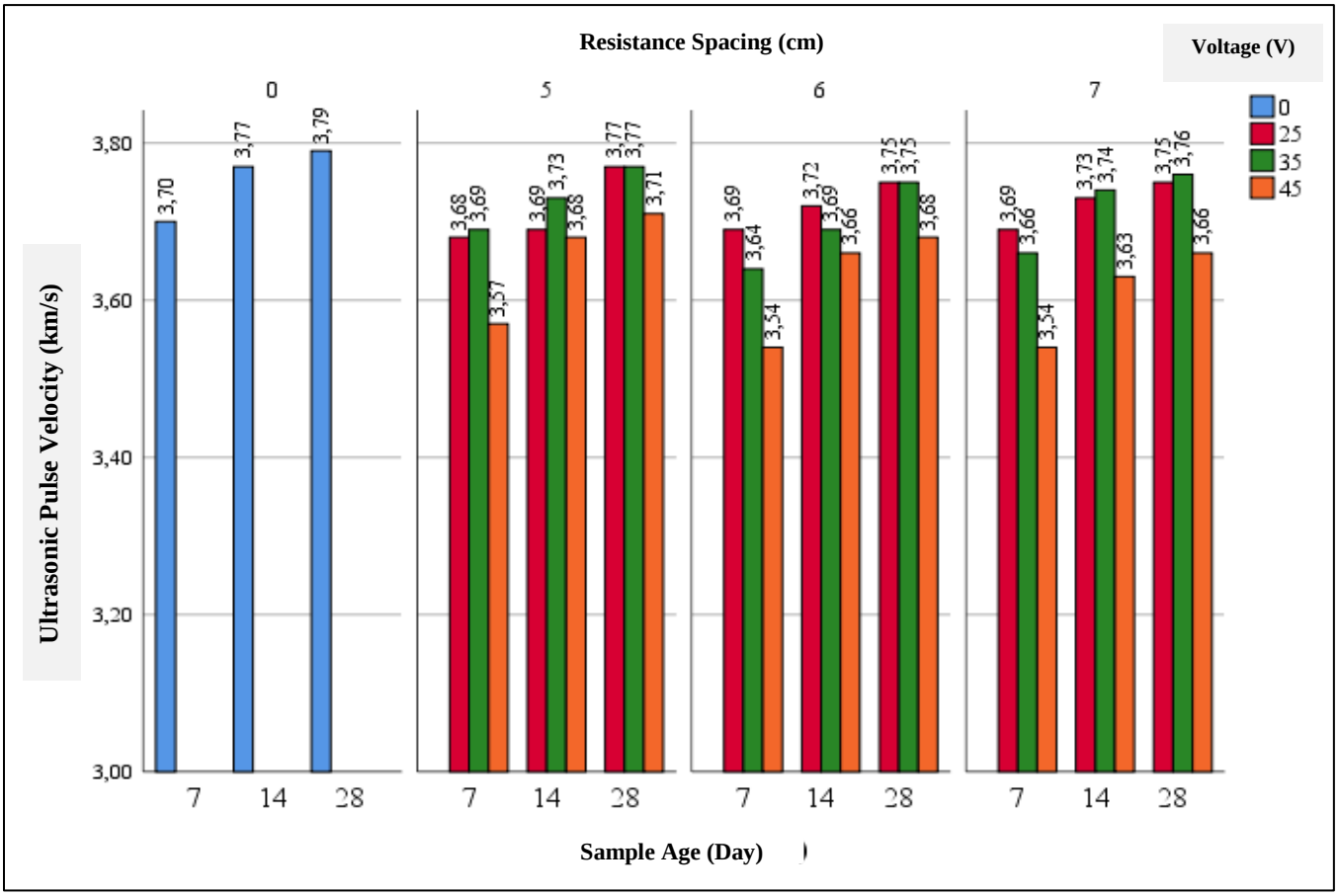

Figure 15. Ultrasonic pulse velocity test data

Flexural strength test results

The results of the flexural strength test conducted on the prepared prism samples are shown in Figure 16.

Upon examining the results presented in Figure 16 it is observed that the flexural strengths of all samples increased with age. For the reference sample, there was a 17.1% increase in strength from day 7 to day 28. This increase was observed in the following samples: CTB-5C-25V (22%), CTB-6C-25V (21%), CTB-7C-25V (19%), CTB-5C-35V (20%), CTB-6C-35V (12%), CTB-7C-35V (30%), CTB-5C-45V (19%), CTB-6C-45V (24%), and CTB-7C-45V (19%). It is evident that the flexural strength increases proportionally with the age of the concrete. Both early-age and later-age samples cured with a 35V current exhibited higher flexural strengths compared to the reference sample. Although samples such as CTB-25V and CTB-45V showed lower values compared to the reference sample on day 7, they demonstrated relatively higher strengths on day 28. In light of these data, CTB-5C-35V and CTB-7C-35V samples exhibited higher flexural strengths compared to the other samples.

The method of curing with electrical resistance heating has been shown to reduce the setting time of concrete (Nie et al., 2016). As a result, samples that set early reached the expected strengths in shorter times and exhibited higher flexural strength values compared to samples that were not cured at early ages.

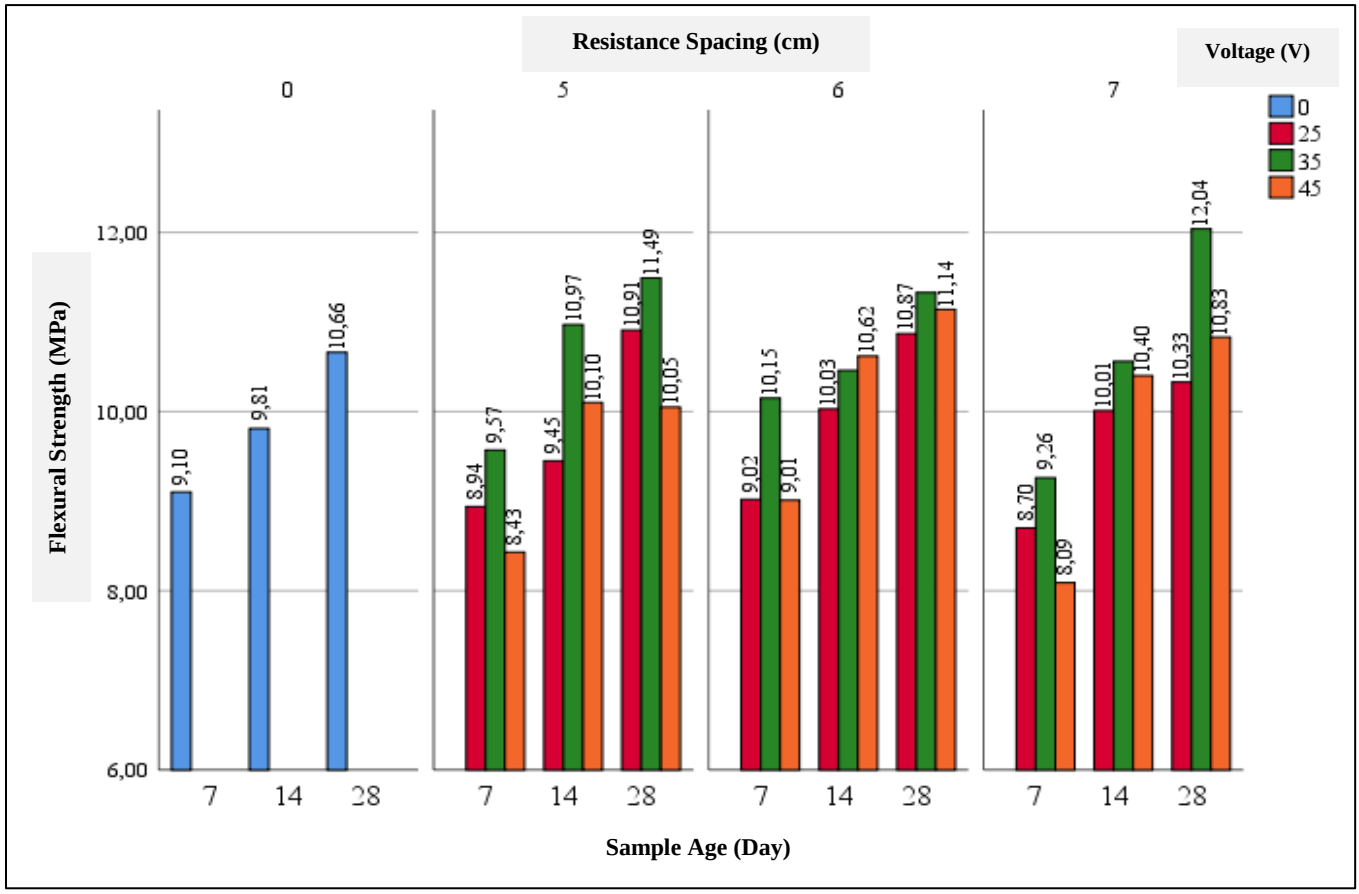

Figure 16. Flexural strength test data

Compressive strength test results

The results of the compressive strength test are shown in Figure 17. Upon examining the compressive strength results of the concrete series, it is observed that the reference sample exhibited lower compressive strength at early ages compared to all other samples except for CTB-25V. However, at later ages, the reference sample showed higher compressive strength. For the 7-day samples, the lowest values were recorded for CTB-5C-25V (34.93 MPa) and the reference sample (35.67 MPa). The highest compressive strength at 7 days was observed in the CTB-6C-45V series (39.73 MPa). The CTB-5C-35V series, which previously provided optimal results in non-destructive tests, achieved the fourth highest compressive strength value after the series cured with 45V current. The CTB-6C-45V series, which provided the maximum strength result, achieved a compressive strength 11% higher than the reference sample. The CTB-5C-35V sample also exhibited a compressive strength 8% higher than the reference sample.

Considering the results on day 14, the reference sample showed a significant increase in strength compared to samples cured with the internal resistance method. On day 14, the reference sample achieved a strength value of 45.14 MPa, which represents a 26% increase compared to its strength on day 7. The CTB-5C-45V series provided the closest value to the reference sample, with a compressive strength of 43.78 MPa, which is 3% lower than the reference sample.

By the end of the 28th day, the reference sample achieved a compressive strength of 52.61 MPa, which represents a 16% increase compared to its strength on day 14. The reference sample had 17% higher compressive strength compared to the CTB-5C-25V sample, which showed the lowest value among the internally cured samples at 44.88 MPa. The samples with compressive strengths closest to the reference were CTB-5C-45V (49.35 MPa), CTB-6C-45V (48.94 MPa), and CTB-5C-35V (48.44 MPa).

The obtained compressive strength results show similarities with the unit weight and ultrasonic pulse velocity values.

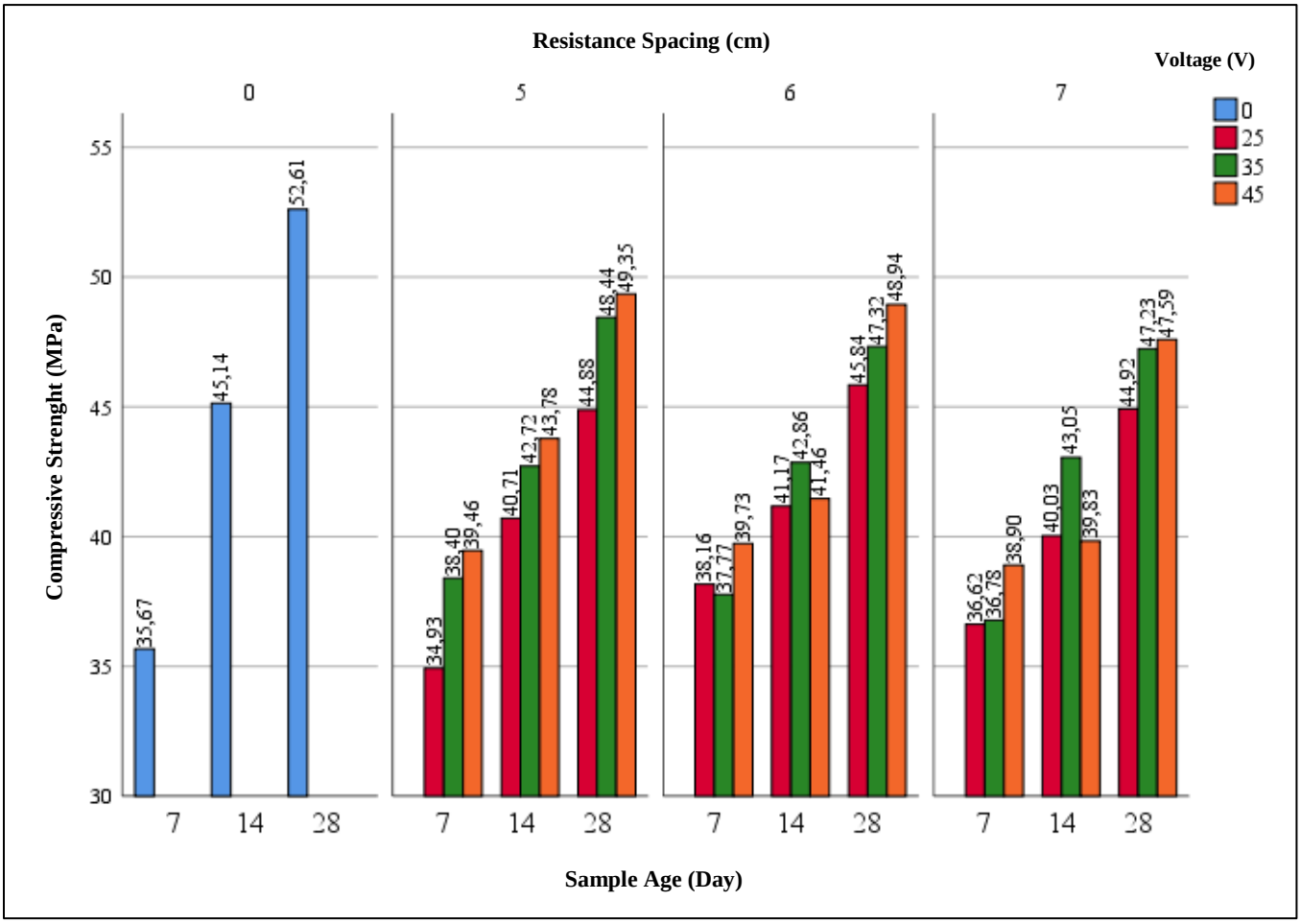

Figure 17. Compressive strength test data

Thermal camera data results

To monitor the temperature changes of internally heated CTBs (Concrete Test Beams), a thermal camera system was set up for all sample specimens. Temperature variations and thermal camera images were recorded at five different time intervals. For specimens cured with internal resistance heating and subjected to electrical currents of 25V, 35V, and 45V, three different molds with wire placements at intervals of 5 cm, 6 cm, and 7 cm were used, and all three molds were subjected to thermal measurement together. Measurements for the REF, CTB-25V, CTB-35V, and CTB-45V series were taken at 0 hours (post-concrete pouring), 4 hours, 8 hours, 12 hours, and 24 hours. The visual representation of the thermal camera measurements for all concrete series is shown in Figure 18. In Figure 18 the thermal camera images and temperature values for the REF, CTB-25V, CTB-35V, and CTB-45V series at 0 hours, 4 hours, 8 hours, 12 hours, and 24 hours are presented together.

Reference series thermal camera measurement results

Since no curing was applied to the reference sample, it was recorded independently in the monitoring system. Thermal camera setups for the reference sample, as shown in Figure 19 were established and monitored over a 24-hour period.

A thermal image was captured immediately after placing the concrete into the mold, at the onset of the setting process, marked as "0 minutes." As shown in the image, with the ambient temperature around 20 °C, the surface temperature of the concrete was 18.6 °C. Temperature changes are expected to be faster and more variable in the first 12 hours; therefore, four images were taken between 0-12 hours, and one image was taken at 24 hours.

Time (Hours)	REF	CTB-25V	CTB-35V	CTB-45V
0 h	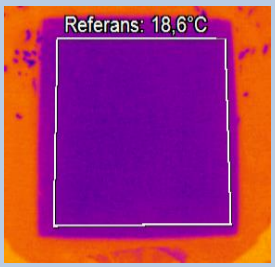 a)	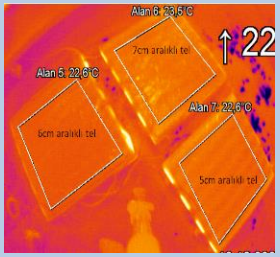 f)	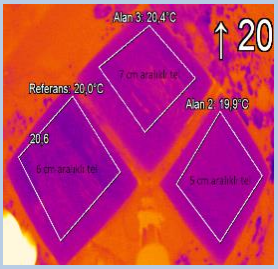 j)	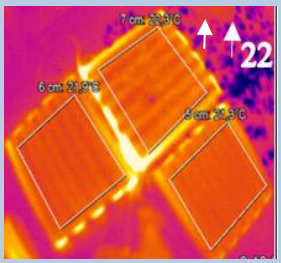 o)
4 h	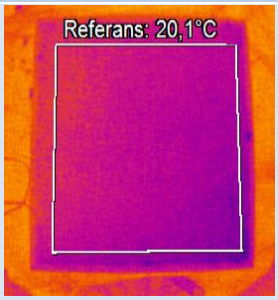 b)	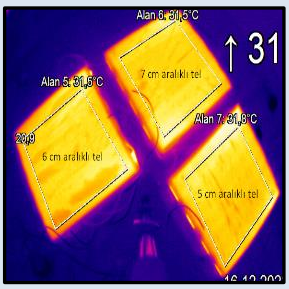 g)	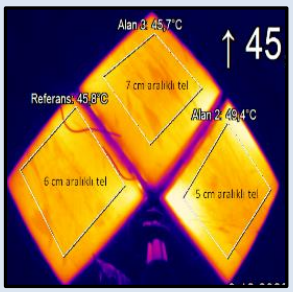 k)	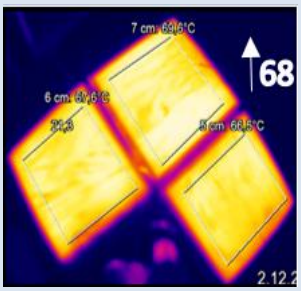 p)
8 h	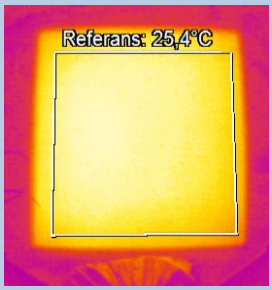 c)	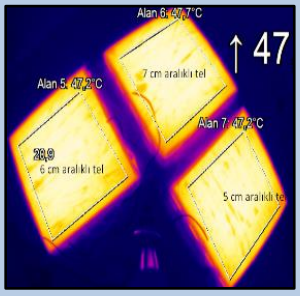 h)	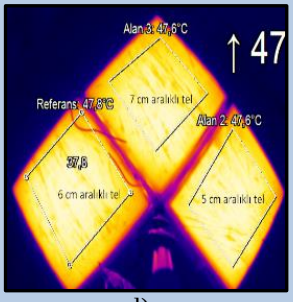 l)	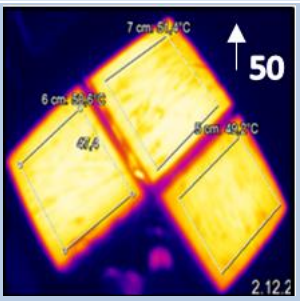 r)
12 h	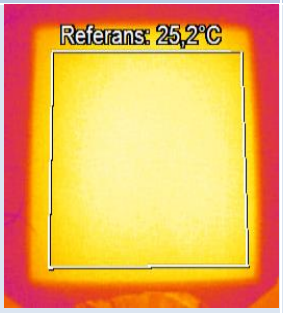 d)	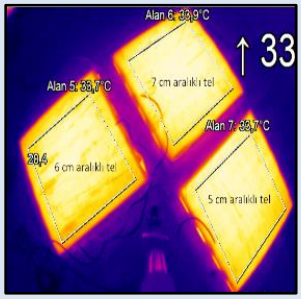 ı)	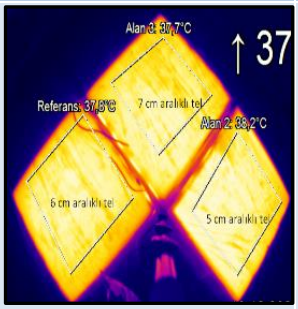 m)	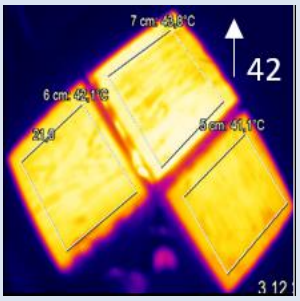 s)
24 h	 e)	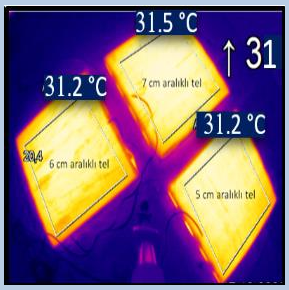 i)	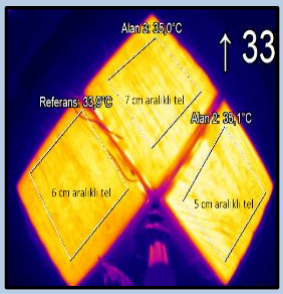 n)	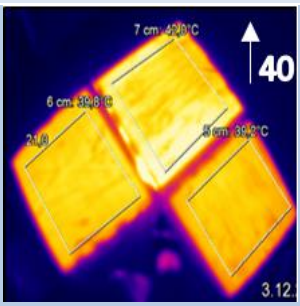 ş)

Figure 18. Thermal camera ımages and concrete surface temperatures

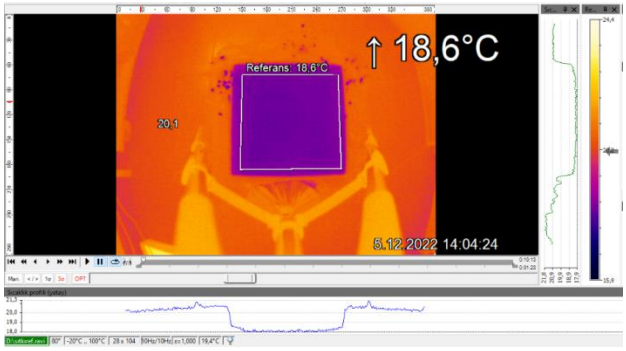

Figure 19. Thermal camera data obtained after concrete pouring (0 h).

The temperature values of the reference concrete sample at the 4th hour after being placed into the mold are shown in Figure 20. Due to the combined effects of ambient temperature and the gradual onset of setting, hydration heat has emerged, raising the surface temperature of the cement by approximately 1.5°C from the initial value. The thermal image and data of the reference sample at the 8th hour of the setting process after being placed into the mold are shown in Figure 21. By the end of the 8th hour, the setting process accelerated, and it was observed that the surface temperature of the cement had increased significantly. The temperature at the end of the 8th hour was approximately 37% higher compared to the initial setting and about 26% higher compared to the temperature at the 4th hour.

The thermal image and data of the reference sample at the 12th hour of the setting process after being placed into the mold are shown in Figure 22. The surface temperature of the reference sample stabilized between the 8th and 12th hours. After reaching its peak, the surface temperature of the cement decreased slightly. The cement transitioned from a fluid to a solid state. By the end of the 12th hour, the surface temperature had decreased by approximately 0.8% compared to the 8th hour.

The thermal image and data of the reference sample at the 24th hour of the setting process after being placed into the mold are shown in Figure 23. After 24 hours, the thermal measurements of the reference sample showed that the temperature remained stable at approximately 23.2 °C. Temperature changes were more rapid within the first 12 hours following concrete pouring, while after 12 hours, the temperature changes slowed and stabilized. By the end of 24 hours, the concrete surface temperature increased by 25% compared to the initial pouring temperature, although this final temperature was approximately 9% below the peak value. The temperature-time curve for the reference sample is illustrated in Figure 24.

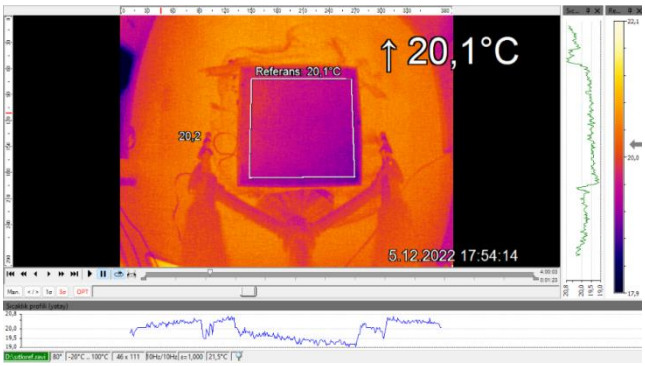

Figure 20. Thermal camera data obtained 8 hours after concrete pouring (4 h).

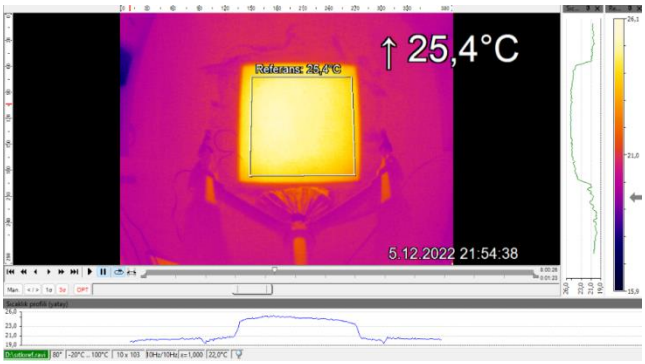

Figure 21. Thermal camera data obtained 8 hours after concrete pouring (8 h).

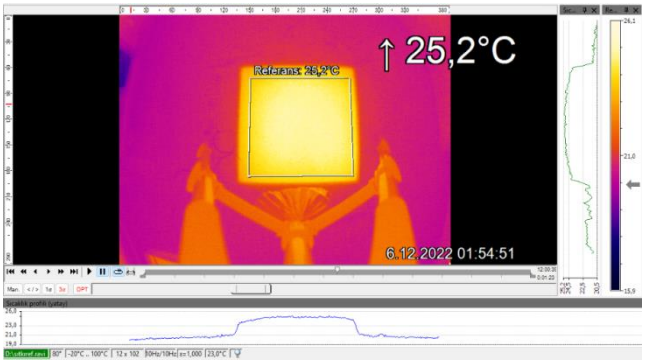

Figure 22. Thermal camera data obtained 12 hours after concrete pouring (12 h).

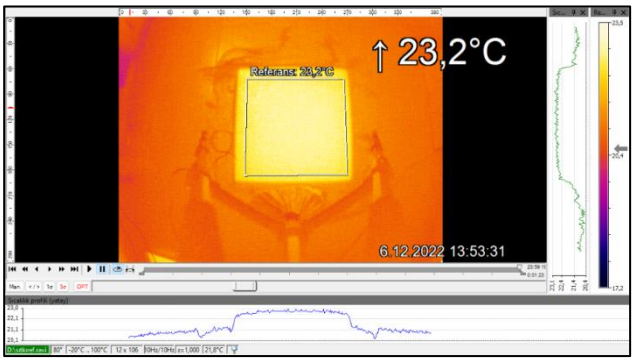

Figure 23. Thermal camera data obtained 24 hours after concrete pouring (24 h).

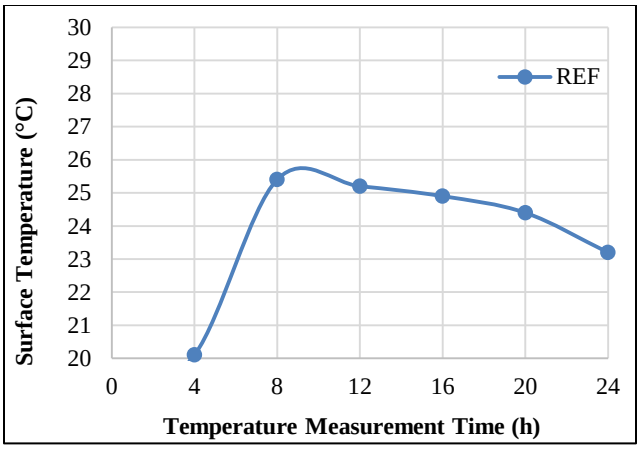

Figure 24. Time-Dependent concrete surface temperature variation curve.

Following the initial concrete pouring, the cement temperature increased over time due to the rise in hydration heat. The sample reached its maximum temperature between 8 and 12 hours, after which it began to lose heat. To prevent the reference sample from being affected by temperature fluctuations, it was kept at a constant room temperature. Otherwise, temperature fluctuations could induce stresses within the concrete, leading to cracks and a reduction in strength. There is a relationship between the increase in concrete temperature and its mechanical strength. While temperature increases can enhance strength in the short term, prolonged exposure to high temperatures may result in a weakened structure over the long term (Mathews et al., 2021).

CTB-25V series thermal measurement results

Concrete slabs cured using the internal resistance method were cured by applying current at three different voltages. Since a single power source was used, the series with different voltage currents were cast on different days. In this series, current was transmitted to the conductive wires for 24 hours. To prevent moisture loss from the concrete slab, the mold was tightly sealed with plastic wrap. The surface temperature of the concrete samples subjected to 25 volts of electrical current before setting is shown in Figure 25. The wire spacing on the molds was specified, and the conductive wires of the three concrete molds were connected in parallel to receive the same voltage from the power source. This initial image was recorded immediately after the setup was completed and electrical transmission began. The temperature values recorded at the end of the 4th hour for the three different samples subjected to a 25-volt current are shown in Figure 26.

After 4 hours, no significant difference was observed in the concrete temperatures within the three molds. The molds with wires spaced at 7 cm and 6 cm intervals had a temperature of 31.5°C, while the concrete in the mold with wires spaced at 5 cm intervals was slightly warmer at 31.8°C, showing a 1% higher temperature compared to the other samples. The laboratory environment where the thermal measurements were conducted maintained a constant temperature of 20.1°C.

The temperature data recorded at the end of the 8th hour for the concrete samples subjected to a 25-volt current are shown in Figure 27.

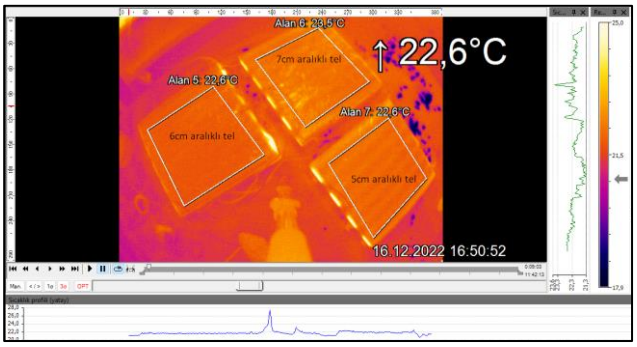

Figure 25. Thermal camera data obtained after concrete pouring (0 h).

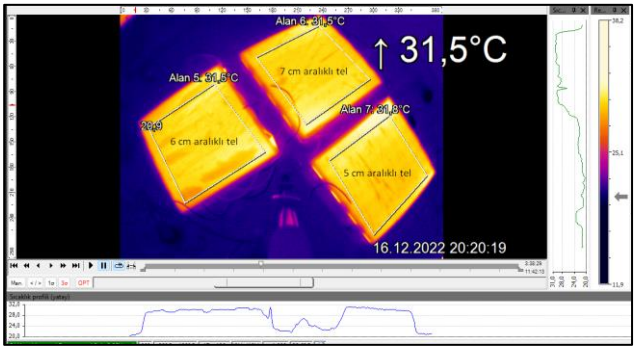

Figure 26. Thermal camera data obtained 4 hours after concrete pouring (4 h).

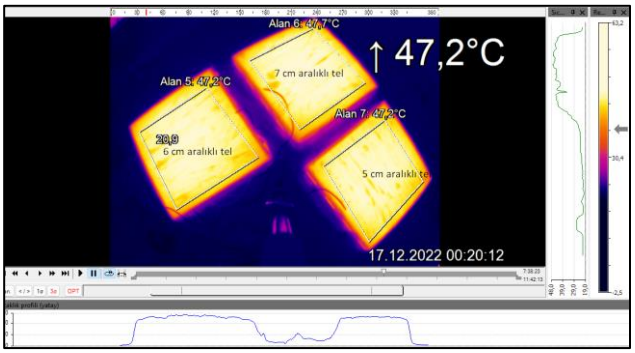

Figure 27. Thermal camera data obtained 8 hours after concrete pouring (8 h).

When examining the figure, it is evident that the series CTB-7C-25V reached the highest temperature. The temperature values of the CTB-5C-25V and CTB-6C-25V series were both 47.2°C. The CTB-7C-25V series was found to have a temperature that was 13% higher than the other series. In these series, the temperature peaked by the end of the 8th hour.

In terms of mechanical tests, no significant differences were observed among the series subjected to 25V current. While early-age temperature increases appear beneficial for mechanical tests compared to the reference sample, it has been found that higher temperatures can negatively affect the strength at later ages.

The temperature data recorded at the end of the 12th hour for the concrete samples subjected to a 25-volt current are shown in Figure 28. After reaching peak temperatures at the 8th hour, the temperatures began to decrease by the 12th hour. Considering the temperature values, it was observed that the temperature changes and values for the CTB-5C-25V and CTB-6C-25V series were the same, both at 33.7°C. The temperature value for the CTB-7C-25V series was slightly higher at 33.9°C, which is 0.6% higher than the other series.

The temperature data recorded at the end of the 24th hour for the concrete samples subjected to a 25-volt current are shown in Figure 29. The concrete within the molds heated by a 25-volt electrical current stabilized at approximately 31-32°C by the end of 24 hours. Since the electrical current was continuously applied beyond the 24th hour, the temperature did not decrease to room temperature. The CTB-7-25V series remained about 1% warmer than the other series.

The temperature-time curve for the concrete series subjected to a 25-volt electrical current is shown in Figure 30.

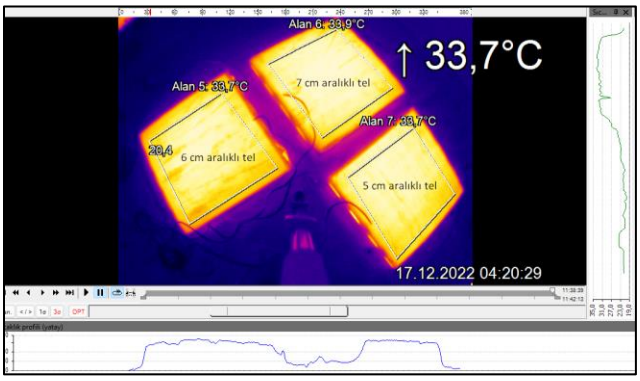

Figure 28. Thermal camera data obtained 12 hours after concrete pouring (12h)

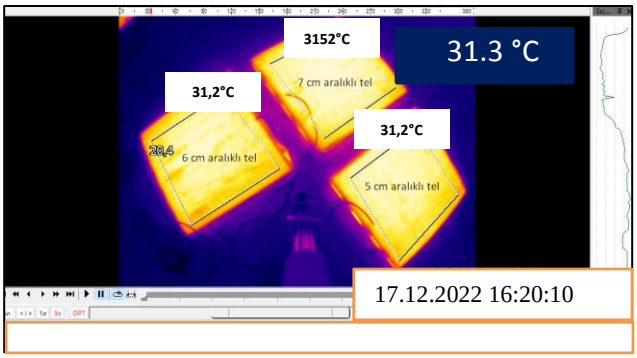

Figure 29. Thermal camera data obtained 24 hours after concrete pouring (24h)

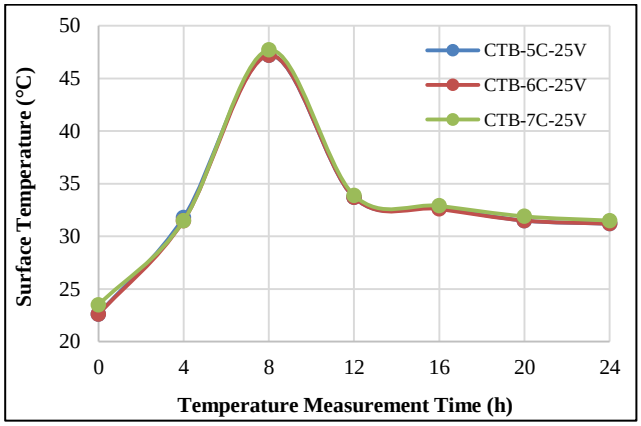

Figure 30. Time-Dependent concrete surface temperature variation curve

As seen in Figure 30, the temperature values for the concrete samples subjected to a 25-volt current were quite similar to each other. Among the concrete series, the CTB-7C-25V sample had a relatively higher temperature compared to the other series. Considering both the temperature values and mechanical test results, the test outcomes were quite close. Although the samples cured using the internal resistance method with 25V electrical current showed positive results at early ages compared to the reference sample, a decline in strength was observed at later ages.

CTB-35V series thermal measurement results

In the curing method where 35 volts of electrical current were applied to the concrete samples, the test results for 0, 4, 8, 12, and 24 hours were analyzed. Figure 31 shows the temperature values for the three concrete series cured with 35 volts of current: CTB-5C-35V, CTB-6C-35V, and CTB-7C-35V.

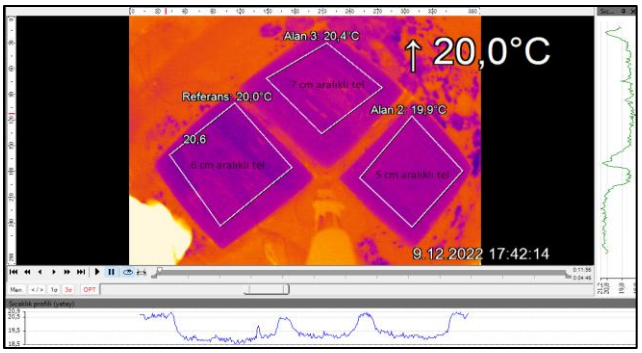

Figure 31. Thermal camera data obtained after concrete pouring (0h).

The temperature values observed after placing the concrete samples into the molds and setting up the thermal camera system are shown in Figure 31. At this stage, since electrical current was also applied, there were temperature differences among the concrete series.

The temperature values of the concrete series subjected to a 35-volt current at the end of the 4th hour are shown in Figure 32.

When examining the surface temperatures of the concrete samples, it is observed that the samples subjected to a 35-volt current had higher temperatures compared to the CTB-25V samples and the reference samples. In Figure 32, it can be seen that the temperature of the CTB-5C-35V sample at the end of the 4th hour was 49.4°C. The surface temperature of the CTB-5C-35V series at this time was found to be 246% higher than that of the reference sample (20.1°C) and 55% higher than that of the CTB-5C-25V sample (31.8°C).

The surface temperature values for the CTB-5C-35V concrete series, obtained from the thermal camera, are shown in Figure 33.

The temperature values of the concrete series cured with a 35-volt current at the 8th hour were found to be quite similar to each other. Comparing the temperatures at the 4th and 8th hours, it was observed that the rate of temperature increase for the CTB-5C-35V sample had slowed compared to the other samples. At this stage, the temperature values for the CTB-5C-35V and CTB-7C-35V series had become similar, while the CTB-6C-35V series was 1% warmer than the other series.

The concrete series subjected to 35 volts exhibited a faster temperature increase compared to the reference and 25-volt series, as evidenced by the temperature differences at the 4th and 8th hours. It has been demonstrated that a faster temperature rise accelerates hydration and shortens the concrete setting time. However, excessive curing duration may lead to both economic and mechanical issues for the samples (Levita et al., 2000).

The temperature values of the concrete series at the end of the 12th hour are shown in Figure 34.

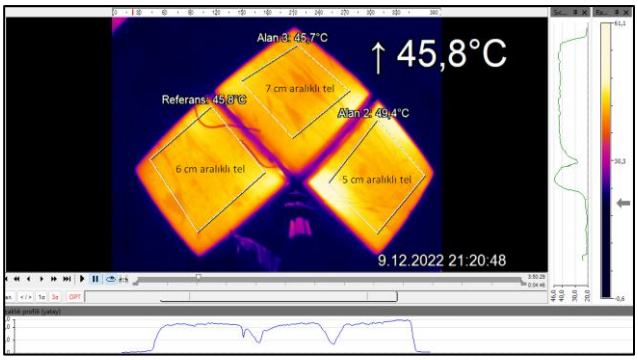

Figure 32. Thermal camera data obtained 4 hours after concrete pouring (4 h).

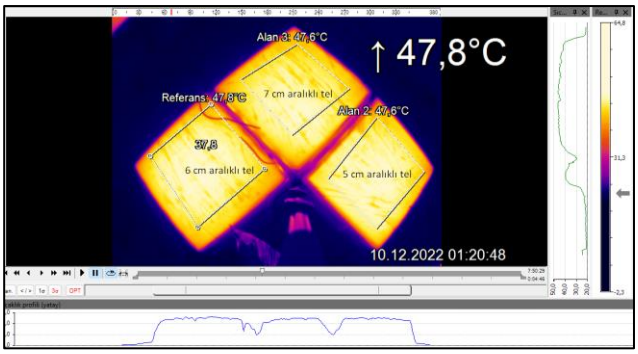

Figure 33. Thermal camera data obtained 8 hours after concrete pouring (8 h).

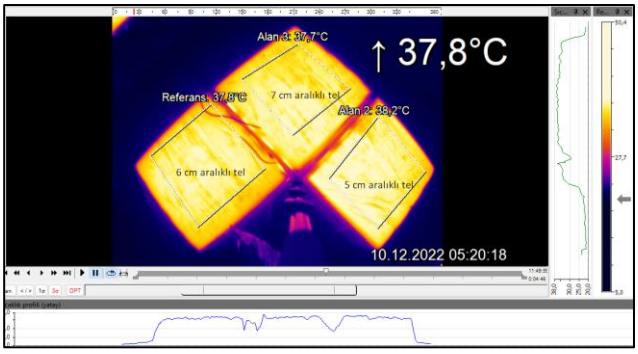

Figure 34. Thermal camera data obtained 12 hours after concrete pouring (12 h).

In the concrete series cured with a 35-volt electrical current, it is observed that the peak surface temperature reached at the 8th hour begins to decrease by the 12th hour. The CTB-5C-35V sample, which had a faster temperature increase compared to other series at earlier hours, was found to cool down more slowly. By the end of the 12th hour, the CTB-7C-35V sample, which had a relatively lower temperature compared to other series, was

1% cooler than the CTB-5C-35V sample. The thermal camera data for the concrete series subjected to a 35-volt current at the end of the 24th hour are shown in Figure 35. At the end of 24 hours of curing with internal resistance, the concrete temperature values were analyzed. Among the three series, the CTB-6C-35V sample was found to cool down the fastest. Conversely, the CTB-5C-35V sample warmed up the fastest and also cooled down the slowest. By the end of the 24th hour, the temperature values were as follows: CTB-5C-35V at 35.1°C, CTB-6C-35V at 33.9°C, and CTB-7C-35V at 35.0°C.

The temperature-time graph for the CTB-35V concrete series is shown in Figure 36. As shown in Figure 36 the temperature values for the CTB-6C-35V and CTB-7C-35V series were close to each other. The CTB-5C-35V sample reached its peak temperature at the 4th hour and was 8% warmer compared to the CTB-6C-35V series, which had the next highest temperature. Over the 24-hour period, the CTB-5C-35V series not only increased its temperature the fastest but also cooled down the slowest. Although there was no significant difference between the other two series, the CTB-6C-35V sample cooled down earlier.

Mechanical tests indicated that the concrete series cured with 35 volts of current provided the most optimal results, closest to the reference sample. The CTB-35V samples, particularly at early ages, exhibited higher and better quality results compared to the reference sample. Concrete samples cured using the internal resistance method with 35 volts showed better flexural strength and ultrasonic pulse velocity results compared to the reference sample. Specifically, the CTB-5C-35V series demonstrated higher mechanical performance in flexural strength at both early and later ages compared to the reference sample. While there were no substantial differences in compressive strength between the two series, the reference sample performed slightly better.

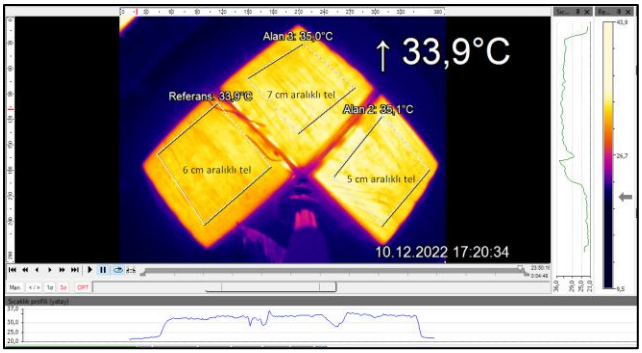

Figure 35. Thermal camera data obtained 24 hours after concrete pouring (24h).

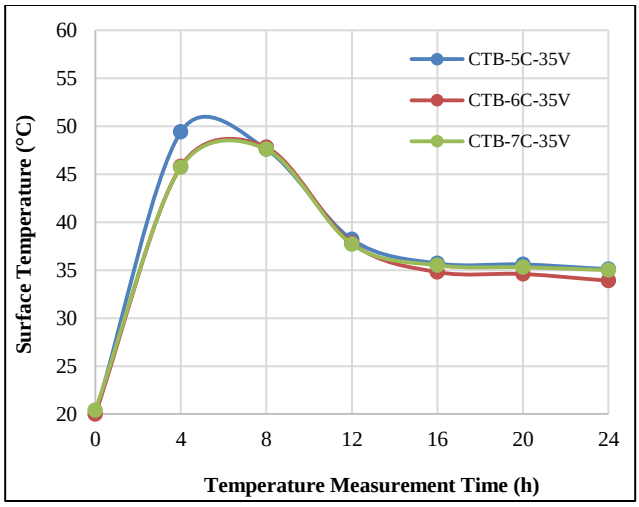

Figure 36. Time-Dependent concrete surface temperature variation curve.

CTB-45V series thermal measurement results

The initial temperature change values of the concrete series subjected to a 45-volt electrical current are shown in Figure 37. The initial images of the concrete series cured with a 45-volt electrical current are provided in Figure 37. The CTB-7C-45V specimen heated up more quickly than the other series after the initial application of the current. In contrast, the CTB-5C-45V specimen exhibited a slower rate of temperature increase compared to the other samples. The temperature change values of the concrete series subjected to a 45-volt electrical current at the end of the 4th hour are shown in Figure 38.

Similar to the initial stage (0 hours), the CTB-7C-45V series heated up more compared to the CTB-6C-45V and CTB-5C-45V series. The CTB-7C-45V series reached a peak temperature of 69.6°C, approximately 5% higher than the CTB-5C-45V series and 3% higher than the CTB-6C-45V sample. It is well known that electrical conduction and high temperatures can affect the microstructure of concrete (Subasi et al., 2022). Experiments have shown that concrete samples reaching very high temperatures during hydration tend to have lower mechanical strength compared to those that reach lower temperatures.

The thermal values obtained at the end of the 8th hour, after the temperature of the concrete series reached its peak, are shown in Figure 39. The thermal camera data of the concrete series subjected to a 45V electrical current at the end of 8 hours were examined. All three specimens, which had reached their peak temperatures, had entered the cooling phase. Similar to the initial and 4th-hour data, a temperature hierarchy was established in the 8th-hour readings. The CTB-7C-45V sample was the hottest, followed by the CTB-6C-45V sample, with the CTB-5C-45V sample having the lowest temperature. The CTB-7C-

45V series, being the hottest specimen, was approximately 5% warmer than the CTB-5C-45V series, the coldest specimen. The data obtained at the end of the 12th hour for the concrete series are shown in Figure 40.

The temperature variations of the concrete samples subjected to a 45-volt current continued in the same order, as shown in Figure 39. The CTB-7C-45V sample remained the hottest, followed by the CTB-6C-45V sample, with the CTB-5C-45V sample maintaining the lowest temperature. The hottest sample, CTB-7C-45V (43.8°C), was approximately 7% warmer than the coldest sample, CTB-5C-45V (41.1°C). The temperature data recorded at the end of the 24th hour for the concrete samples are shown in Figure 41.

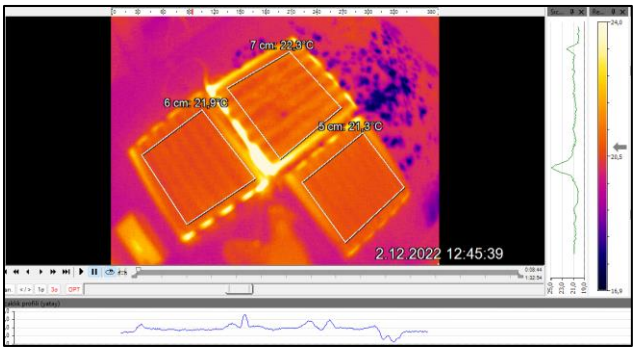

Figure 37. Thermal camera data obtained after concrete pouring (0h).

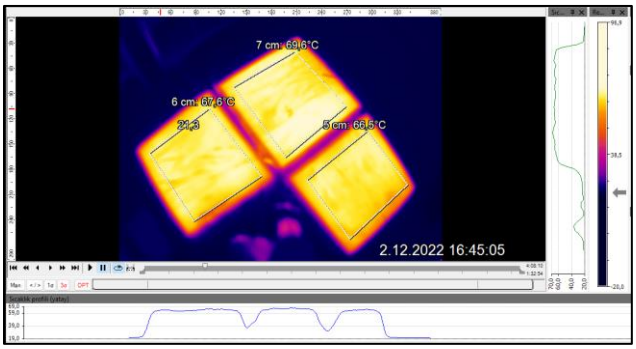

Figure 38. Thermal camera data obtained 4 hours after concrete pouring (4h).

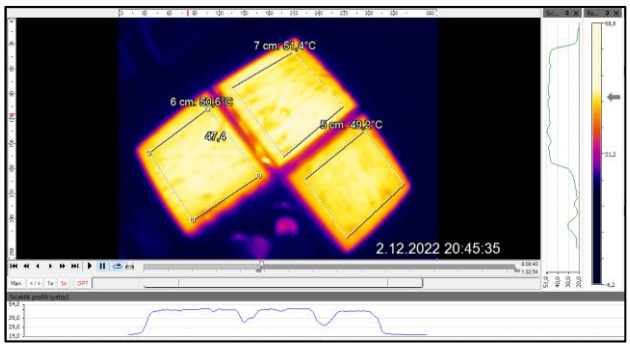

Figure 39. Thermal camera data obtained 8 hours after concrete pouring (8h).

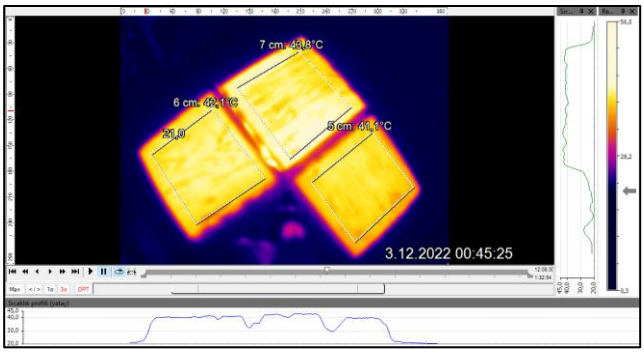

Figure 40. Thermal camera data obtained 12 hours after concrete pouring (12h)

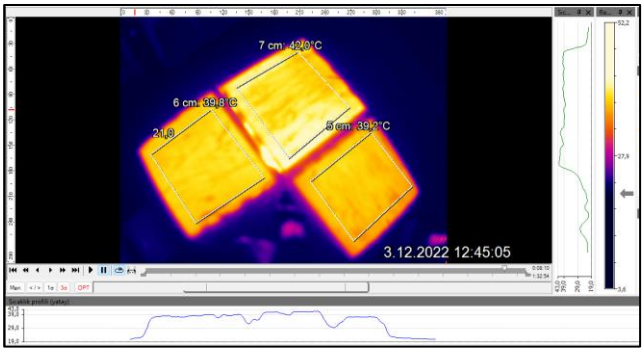

Figure 41. Thermal camera data obtained 24 hours after concrete pouring (24h).

The temperature values of concrete samples after 24 hours of curing with internal resistance were analyzed. Among the three series, the sample CTB-5C-45V exhibited the fastest cooling rate. Conversely, within these three series, the sample CTB-7C-45V demonstrated the fastest heating rate and the slowest cooling rate. At the end of the 24-hour period, the temperatures were as follows: 39.2°C for the CTB-5C-45V series, 39.8°C for the CTB-6C-45V series, and 42°C for the CTB-7C-45V series. Samples subjected to 45 volts of electrical current showed temperature increases of 12%, 17%, and 20%, respectively, compared to those subjected to 35 volts of electrical current.

The temperature-time graph for the CTB-45V concrete series is provided in Figure 42.

As shown in Figure 42, the temperature values of the CTB-5C-45V and CTB-6C-45V series are quite close to each other. Upon examining the graph, it is observed that all series reached a peak temperature and then gradually cooled down before stabilizing. The CTB-7C-45V sample reached a peak temperature of 69.6°C, making it the highest temperature achieved among all series. It was observed that applying 45 volts of electrical current to the conductive wires raised the concrete to significantly high temperatures. When compared to the peak temperature of the reference sample (25.4°C), the CTB-7C-45V series (69.6°C) achieved a temperature increase of 274%. Considering the mechanical tests, it can be inferred that

such high temperatures could negatively impact the concrete's strength.

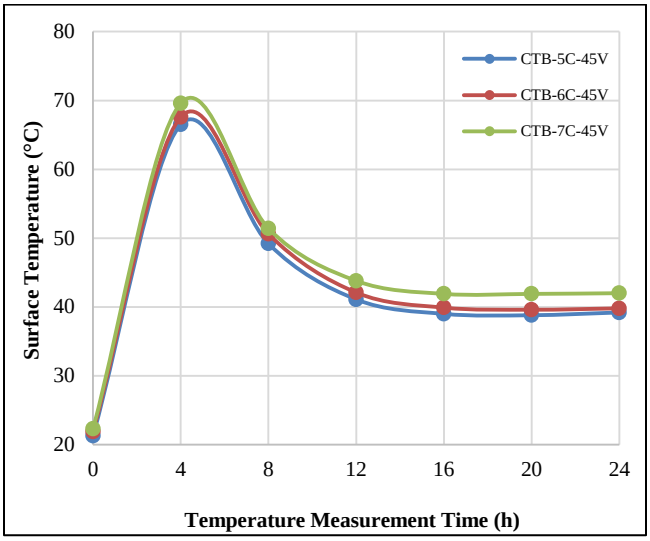

Figure 42. Time-Dependent concrete surface temperature variation curve.

SEM analysis results

The primary objective of SEM analysis is to obtain detailed images of the material's internal structure to gather information about both its physical and chemical composition. This provides insights into the material's characterization at both early and current ages. Figure 43-a shows the SEM image of the reference sample. In Figure , the image magnified at 500× reveals glass fibers. Figure 43-b, magnified at 10,000×, displays the hydration products.

As shown in Figure 43-a), the 500× magnified image reveals C-S-H gels, AR glass fibers, and micro-cracks. The image shows micro-cracks occurring parallel to the fibers. Micro-cracks perpendicular to the fibers are not visible. These parallel cracks, if not addressed at later ages, could negatively impact the durability and physical condition of the sample. The general appearance shows a dense structure. No distinct perpendicular cracks in the fibers were observed, indicating that the AR glass fibers in the sample are effective in preventing vertical cracks (Saran et al., 2007).

In Figure 43-b), the presence of CH (Portlandite) formations alongside C-S-H gel is observed. C-S-H gels cover about 70% of the solid phase of the sample. Both C-S-H gels and CH are key factors affecting the strength of the sample. The hydration products are clearly visible due to the complete chemical reactions in the reference sample. As seen in the figure, C-S-H gels dominate the majority of the image. The analysis shows very few capillary and gel voids, resulting in a high-density appearance. This indicates that the mechanical strength is higher compared to samples cured with internal resistance.

Images of the glass fibers and hydration products of the CTB-5C-25V sample are shown in Figure 44 with magnifications of 500× and 10,000×, respectively.

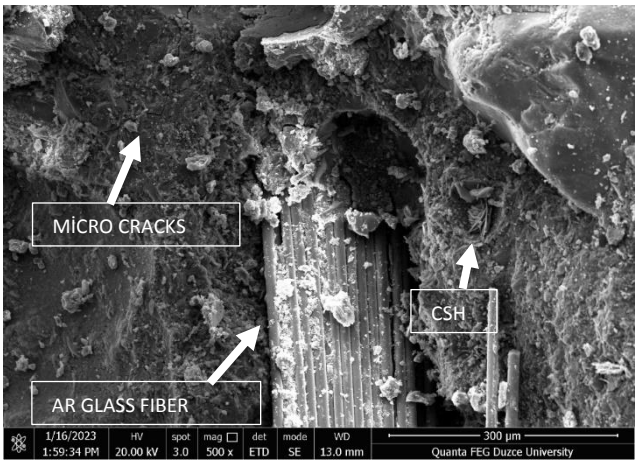

a) 500× magnified image

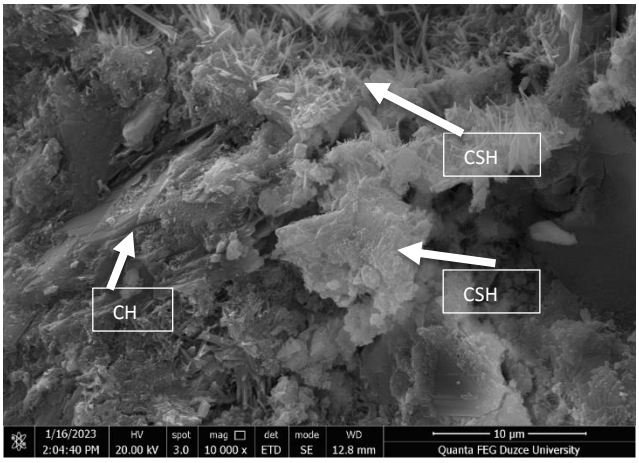

b) 10 000× magnified image

Figure 43. SEM Images of the Reference Sample: a) 500×, b) 10,000× Magnification.

As shown in Figure 44-a), there are parallel and partially perpendicular cracks in the AR glass fibers. These cracks negatively affect the sample's strength. Additionally, it is observed that the products forming the cement matrix do not create a fully homogeneous structure. In Figure 44-b), a porous structure is visible. The image reveals noticeable micro-voids. The presence of these voids indicates that the CTB-5C-25V sample generally yields lower results compared to other samples. Additionally, C-S-H gels, also known as tobermorite, are visible in the image. The presence of tobermorite is related to the dense structure in the microstructure. Compared to the reference sample, the CTB-5C-25V sample exhibits a more porous structure. The lower density and less compact CH (Portlandite) C-S-H structures directly affect the strength, resulting in higher strength values for the reference sample. Furthermore, the lower unit weight test results of the CTB-5C-25V sample compared to other

samples have been attributed to the size and quantity of the micro-voids.

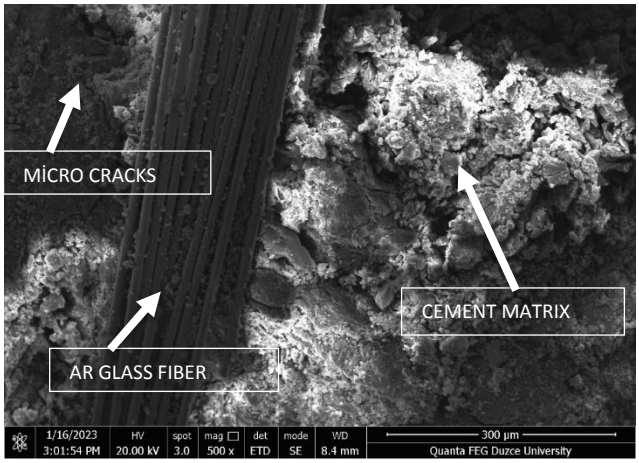

a) 500× magnified image

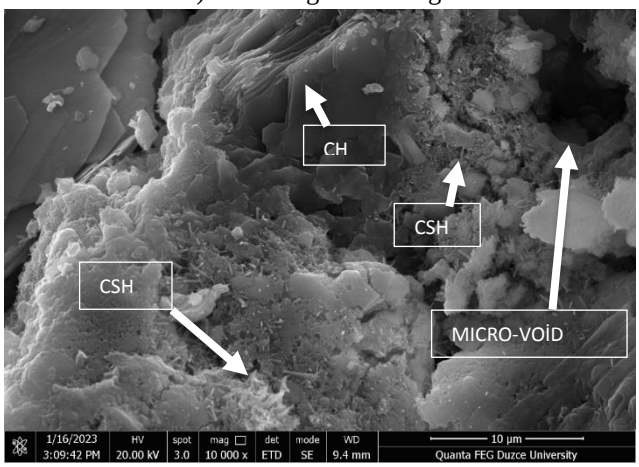

b) 10 000× magnified image

Figure 44. SEM Images of the CTB-5C-25V Sample: a) 500×, b) 10,000× Magnification.

Figure 45 shows SEM analysis images of the CTB-5C-35V sample at different magnifications. The two images provided (a and b) are magnified at 500× and 10,000×, respectively. Figure 45-a) shows the microstructure image of the CTB-5C-35V sample at 500× magnification. The image displays particles of various sizes and shapes. The analysis reveals that the surfaces are generally rough, indicating a potential for good bonding and adhesion. No significant macrostructural cracks are observed in the image, suggesting that AR glass fibers are effective in preventing vertical cracks. Some pore structures are visible in the image. The distribution, density, and size of the pores can affect the material's mechanical properties. The non-typical porous structure is likely impeded by the dense aggregate and metakaolin. The observed pores have not significantly impacted the strength of the CTB-5C-35V sample.

In Figure 45-b), a dense appearance is seen in the internal structure of the CTB-5C-35V sample. A small amount of micro-voids is detected, which is less than in the CTB-5C-25V sample but more than in the reference sample. The image shows impermeable, cloudy C-S-H structures. The high density of this gel is a result of the complete chemical reactions among the materials in the sample. This density explains the higher mechanical strength of the sample compared to the CTB-5C-25V sample (Bentz and Paul, 2006). The microstructure analysis shows surface roughness, which contributes to good bonding. The SEM analysis results of the CTB-5C-35V sample indicate that the small micro-cracks and voids observed lead to lower strength at later ages compared to the reference sample.

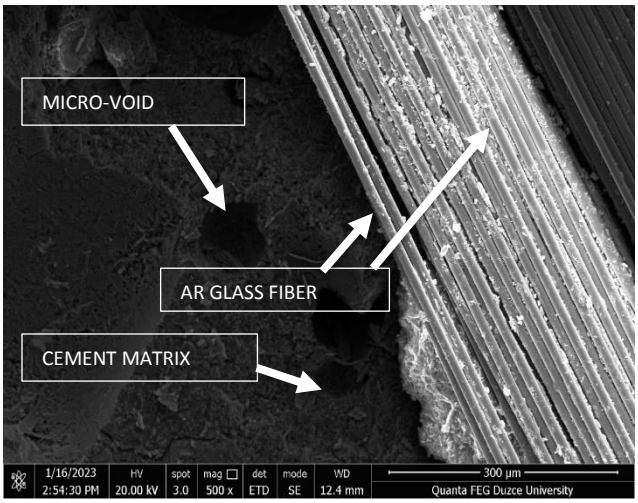

a) 500× magnified image

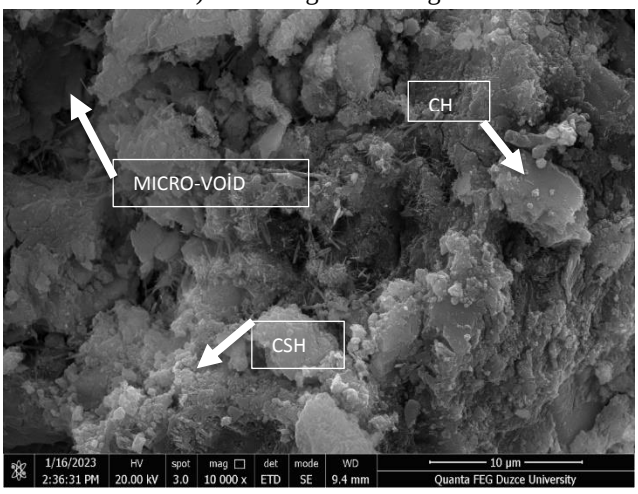

b) 10 000× magnified image

Figure 45. SEM Images of the CTB-5C-35V Sample: a) 500×; b) 10,000× Magnification

Figure 46 presents the SEM analysis images of the CTB-5C-45V sample, which was subjected to the highest voltage. The two images provided (a and b) are magnified at 500× and 10,000×, respectively. Figure 46-a) shows the SEM analysis image of the CTB-5C-45V sample at 500× magnification. The image reveals microstructural cracks developing around the AR glass fibers. These micro-cracks are observed to be parallel to the glass fibers. The image also shows white areas, which are unhydrated cement particles. Additionally, pores have formed within the sample. These pores are found to result from chemical shrinkage and rapid setting during hydration (Sallı Bideci et al., 2017. Compared to other samples, the ultrasonic pulse velocity and flexural strength data for the CTB-5C-45V sample are lower.

Figure 46-b) presents the SEM analysis image of the CTB-5C-45V sample at 10,000× magnification. The image highlights microstructural cracks, gel voids, and micro-voids. In cases where the bonds between cement particles and aggregate are relatively weak, micro-cracks at the interface between the cement paste and aggregate are observable (Doğan et al., 2023). These micro-cracks explain the decrease in flexural strength of the concrete sample heated with 45 volts of electrical current. It is reported that the silica sand used as aggregate in the sample fills the pores, reduces $Ca(OH)_2$ components, and converts $Ca(OH)_2$ crystals into C-S-H structure (Puertas,. Despite the increased surface and internal temperature of the concrete due to high voltage application, the proportion of silica sand in the mix has prevented excessive increase in pore size in the matrix and contributed to the densification of the structure. CH (Portlandite) and C-S-H structures are also visible in the microstructure, which explains the high compressive strength of the CTB-5C-45V sample.

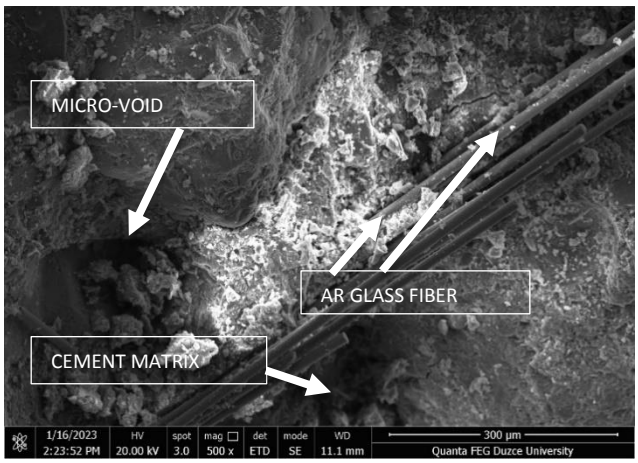

a) 500× magnified image

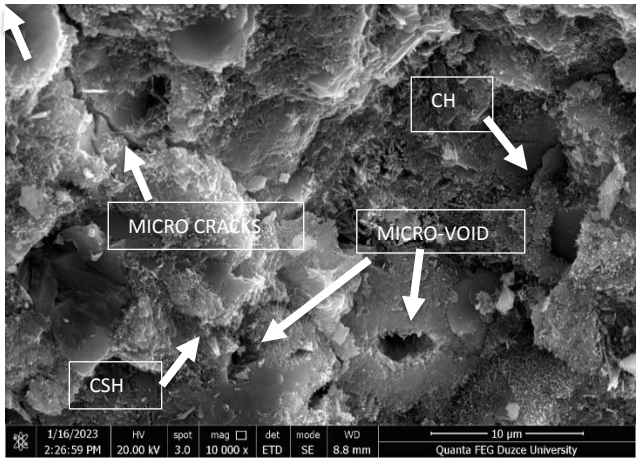

b) 10 000× magnified image

Figure 46. SEM Images of the CTB-5C-35V Sample: a) 500×; b) 10,000× Magnification

TGA (thermogravimetric analysis) results

TGA measurements were conducted for the thermal degradation and weight loss of all concrete samples. Differential Thermal Analysis (DTA) was used to detect the thermal degradations of the samples, and the resulting weight losses were measured with TGA. This analysis investigated the effects of varying voltage-temperature and resistance distance applied to the concrete through resistance wires on the material.

TGA results for CTB-25V series

Figure 47 shows the TGA results for the CTB-25V and REF series, including multiple curves.

Figure 47 shows the TGA and DTA results for the CTB-25V and REF series. The impact of temperature application on the mass losses of the samples was determined. The observed mass losses for all series in the temperature range of 24°C to 129°C were approximately 6%. The CTB-25V and REF series showed very similar values within this range. The CTB-6C-25V series experienced slightly lower mass loss (5.30%) compared to the other series. This mass loss was due to the evaporation of water and volatile components in the sample. The second major mass loss occurred around 436°C. While the mass loss rate was low between 24°C and 129°C, it increased between 436°C and 722°C. The CTB-7C-25V series experienced the highest mass loss during this period. The mass losses observed were attributed to the thermal decomposition of organic compounds within the sample. No significant mass loss was observed after raising the temperature from 756°C to 910°C, with all series retaining

approximately 80% of their mass. This indicates the presence of thermally stable compounds.

Among the concrete series, the CTB-7C-25V sample had the highest mass loss at 19.87%. The REF and CTB-5C-25V series had mass losses of 16.92% and 17.30%, respectively, showing close values. The CTB-6C-25V sample had the lowest mass loss at 16.59%. The DTA results were consistent with the TGA measurements, with the primary mass loss observed between 436°C and 722°C.

TGA results for CTB-35V series

Figure 48 shows the multiple curves of TGA results for the CTB-35V and REF series. Figure 3.35 shows the TGA and DTA results for the CTB-35V and REF samples. According to the results, the temperature application affects the mass losses of the samples. Examining the weight losses, it is observed that approximately 6-8% mass loss occurs across all series in the range of 24°C to 129°C. The CTB-7C-35V sample experienced the highest mass loss (%7.93) in this range, while the CTB-5C-35V sample showed the lowest mass loss (%5.80). The weight losses occurring at lower temperatures (24°C and 129°C) are due to the evaporation of water molecules in the sample. The second mass loss is observed at around 436°C. The analysis of the CTB-35V series reveals a graph quite similar to the results shown in Figure 47 for the CTB-25V concrete series. However, in this case, the REF sample experienced the highest mass loss in the 24°C to 129°C range. Compared to the CTB-25V samples, the CTB-35V samples were exposed to higher temperatures during the internal resistance curing stage, resulting in differences in weight loss between the two series due to the evaporation of water molecules in the 24°C to 129°C range. In all series, the mass loss rate was low in the 24°C to 129°C range, but it increased in the 436°C to 722°C range. Initially, the REF sample had the lowest mass loss rate, but in the 436°C to 722°C range, the CTB-7C-35V series experienced the greatest increase in mass loss, with CTB-7C-25V showing the highest mass loss (%17.30). This was followed by the reference sample with a mass loss rate of %16.06. No significant mass loss was observed after 722°C. Although the CTB-5C-35V and CTB-6C-35V series showed quite similar values, the CTB-5C-35V series had the lowest mass loss (%13.84) when the temperature reached 1000°C. The endothermic peaks in the DTA graph are consistent with the TGA data.

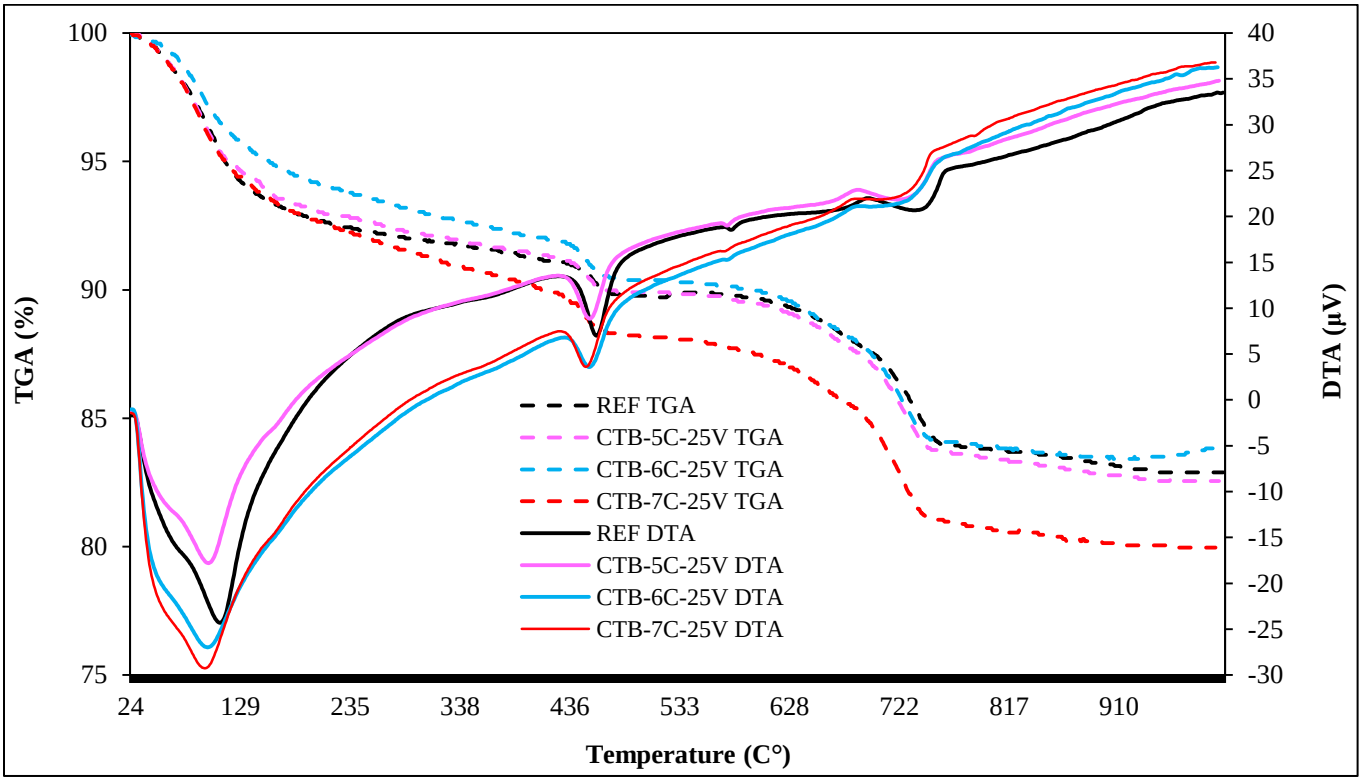

Figure 47. Presents the TGA and DTA result graphs for the CTB-25V and REF concrete series.

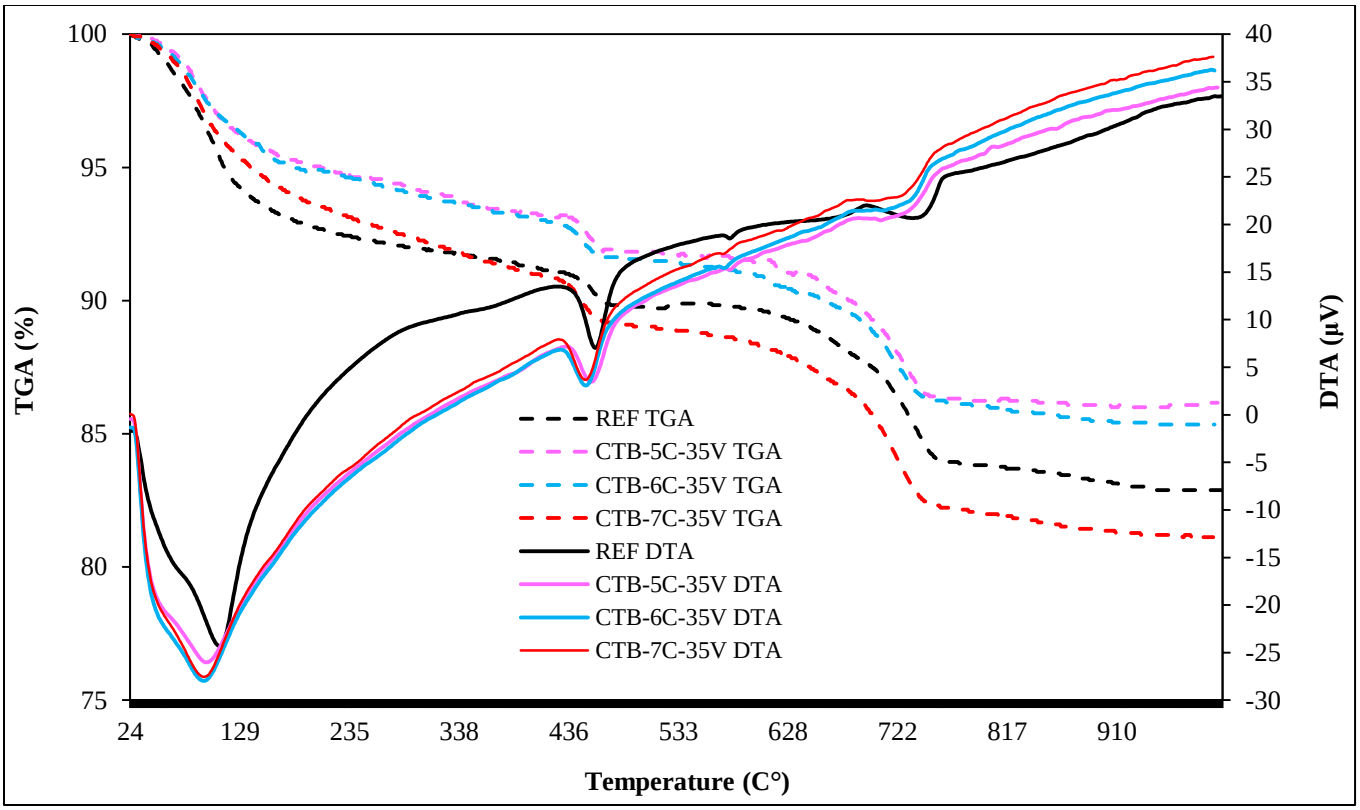

Figure 48. Presents the TGA and DTA result graphs for the CTB-35V and REF concrete series.

TGA Results For CTB-35V Series

Figure 49 shows the TGA and DTA results for the CTB-35V and REF series. Figure 49 shows the TGA and DTA results for the CTB-45V and REF samples. The results indicate that the temperature application affected the mass losses of the samples. Mass losses observed in the range of 24°C to 129°C across all series ranged approximately from 3% to 8%. The CTB-45V and REF series yielded results that were more distant from each other compared to the CTB-25V and CTB-35V series in this range. When the voltage intensity applied to the concrete sample was increased during internal resistance curing, the potential mass loss difference at low temperatures increased with the REF sample. The REF sample experienced the highest mass loss (%7.32) in the 24°C to 129°C range. The CTB-5C-45V and CTB-6C-45V series showed the lowest mass losses with rates of %4.66 and %4.80, respectively. The mass losses occurring at lower temperatures (24°C and 129°C) are due to the evaporation of water molecules in the sample. The second mass loss was observed at 436°C, consistent with the second peak point in the DTA graph. These distinct peaks indicate phase changes or the occurrence of chemical reactions. The analysis of the CTB-45V series revealed a graph quite similar to those for the CTB-25V and CTB-35V concrete series shown in Figures 47 and 48 The distribution of mass loss in the 24°C to 129°C range was identical for the CTB-35V and CTB-45V series. Similar to the previous CTB-25V and CTB-35V series, the CTB-45V graph also showed that the rate of mass loss increased slowly in the 24°C to 129°C range but accelerated in the 436°C to 722°C range. After reaching 722°C, the mass loss partially stabilized at the third peak point in the DTA graph. When examining the mass losses of the CTB-25V, CTB-35V, and CTB-45V graphs after 722°C, it is observed that the mass loss for the CTB-7C series approaches that of the REF sample in proportion to the applied voltage. At 1000°C, the highest mass loss was observed in the CTB-7C-45V series with a rate of %18.3. The CTB-6C-45V sample had the lowest mass loss at %13.84. The DTA and TGA graphs are consistent, with peak points aligning with each other.

Comparison of TGA results for CTB-5C and REF series

The TGA results for the CTB-5C series and the REF sample are presented in Figure 50. The graph in Figure 50 shows the TGA results for the CTB-5C series and the REF sample together for comparison.

In the graph shown in Figure 50, the TGA results of the CTB-5C series and the REF sample are presented together for comparison. The graph reveals that the temperature increase applied during the thermogravimetric analysis affects all series. Between 24°C and 129°C, there is an approximate mass loss of 4-7% due to evaporation. Considering the mass losses in this range, the REF and

CTB-5C-25V values show similar mass losses, while CTB-5C-35V and CTB-45V values also exhibit similar mass losses but at a lower level. In the DTA graph, the first peak occurs at approximately 100°C, while the second peak occurs at approximately 450°C. The mass loss rate increases after the second endothermic peak. After the third peak (750°C), the mass loss stabilizes, with no significant differences observed. At 1000°C, the mass losses were found to be 17.46% for CTB-5C-25V, 17.11% for REF, 14.54% for CTB-5C-45V, and 13.92% for CTB-5C-35V. The DTA and TGA graphs are observed to be consistent with each other.

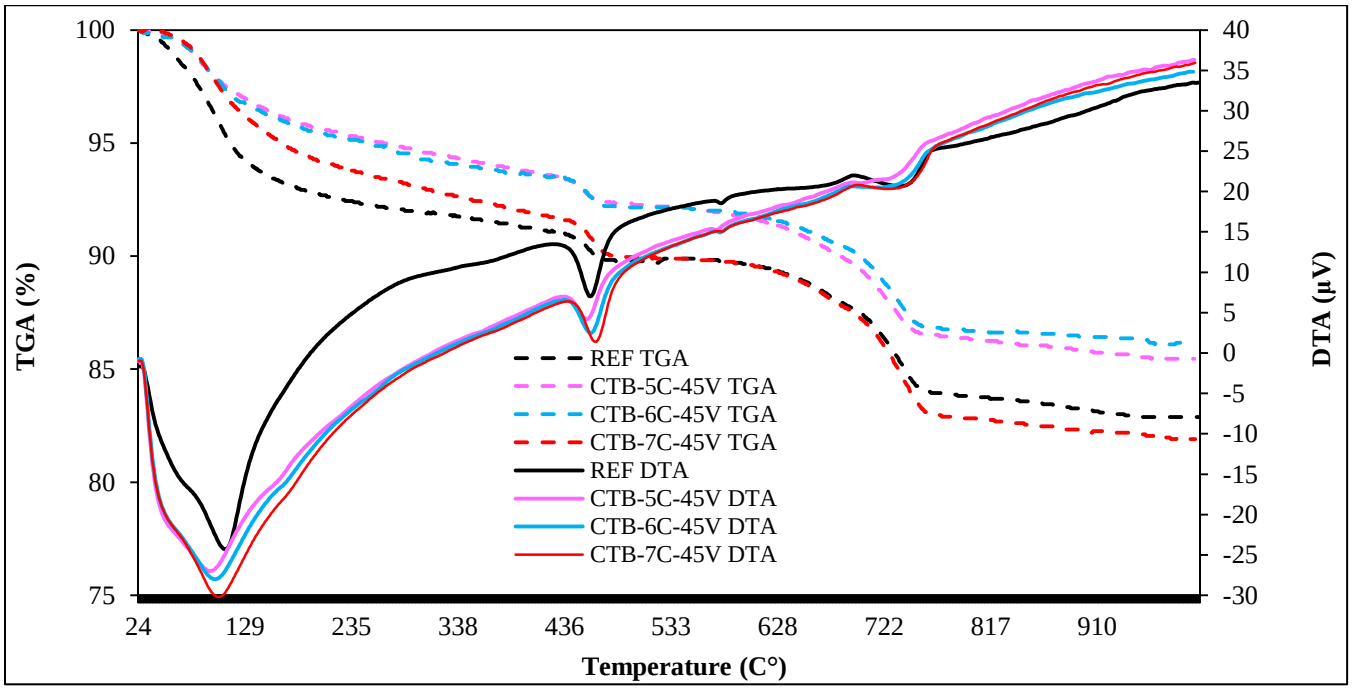

Figure 49. Presents the TGA result graphs for the CTB-35V and REF concrete series.

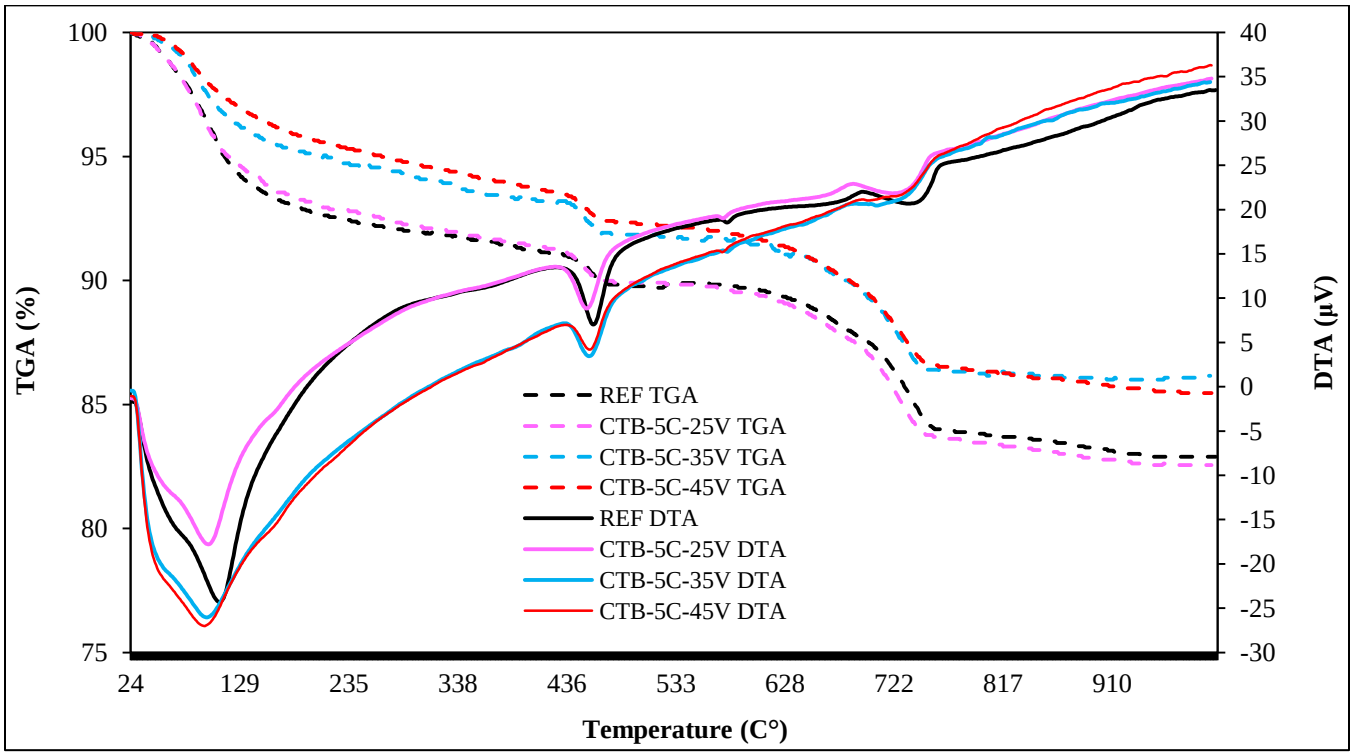

Figure 50. The TGA results graph for the CTB-5C and REF concrete series.

FT-IR (Fourier Transform Infrared Spectroscopy) analysis results

FT-IR analyses were performed on powdered samples of all concrete series. These analyses determined the chemical characterizations of the samples and revealed the effects of voltage differences on the material. According to the infrared spectrum evaluation, FT-IR analysis is primarily assessed in four broad band regions. The frequency peaks are formed based on movements in Si-Al, S, C, and OH bonds, and differences in these wavelengths can be regionally evaluated (Şahin and Koçak, 2022).

In FT-IR analysis, vibrations of the atoms forming solid lattices are observed in the wavelength range of 500-1600 cm^{-1}, while molecular vibrations are monitored in the wavelength range of 1600-3000 cm^{-1} (De and Pereira Gomes, 2005).

FT-IR results of the CTB-25V series

FT-IR analysis results for the CTB-25V series and REF sample are presented in four different spectra in Figure 51.

Figure 51 shows the trend graph containing the FT-IR analyses of the CTB-25V and REF samples. The graph displays multiple peak points. The peaks observed in the graph are within the bands of 4000-3000 cm^{-1}, 3000-2000 cm^{-1}, 2000-1250 cm^{-1}, 1250-800 cm^{-1}, and 800-550 cm-1. The values for all series are quite close to each other. The first peak for all series is within the range of 3700 cm^{-1} and 3500 cm^{-1}. This range indicates the vibrations of OH groups or the presence of hydrated silicates (C-S-H). Upon examining the samples presented in the graph, these wavelengths demonstrate free OH groups or OH groups weakly bound by hydrogen bonds. The peaks formed determine the amount of free water in the cement during the hydration process. In the first peak, the sample CTB-7C-25V, with the highest wave amplitude, was identified with a wavenumber of 3641 cm^{-1}. In the second band area, peaks are observed at wavenumbers of 2400 cm^{-1} and 2000 cm^{-1}. These peak data are associated with CO2 absorption. The higher wavenumber and depth in the first two peaks were observed in the CTB-7C-25V (2374 cm^{-1}) sample. The peaks observed in the third region indicate the presence of water molecules during the cement hydration process. The highest depth in this region was reached by the CTB-5C-25V sample at a wavenumber of 1652 cm^{-1}. The third peaks indicate H-O-H bending vibrations. At points where significant changes are observed, a change occurs in the water content of the cement or the state of bonding. In the fourth peak and vibration point, the CTB-6C-25V sample has a wavenumber of 1074 cm^{-1}. This peak indicates Si-O stretching vibrations. It is observed that silicate structures present in the cement are prominent at this wave amplitude. In the fifth peaks observed at the end of the graph, the vibrations of compounds such as calcium silicates and aluminates are seen. The presence of minerals that constitute the main components of the cement is observed in these peak points. In the fifth peak of the CTB-7C-25V sample, it is understood that the region with the most intense presence of these minerals is at a wavenumber of 551 cm^{-1}.

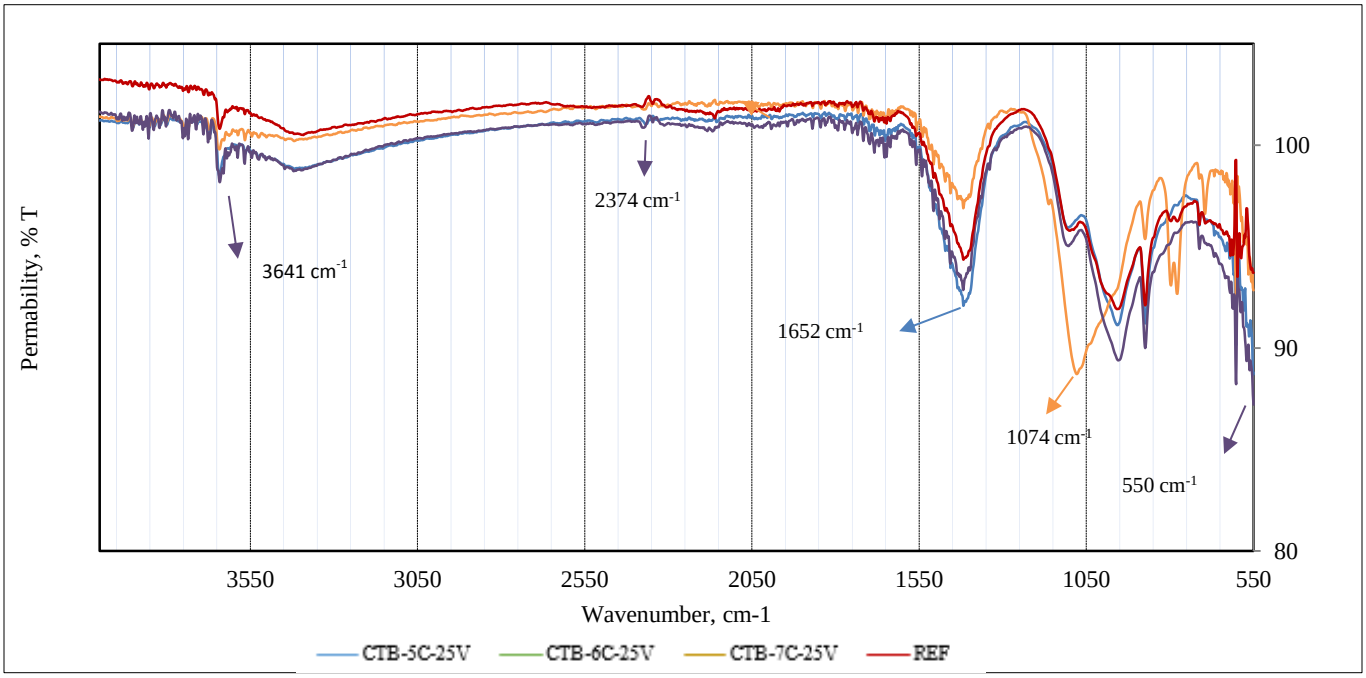

Figure 51. FT-IR results graph for the CTB-25V and REF concrete series

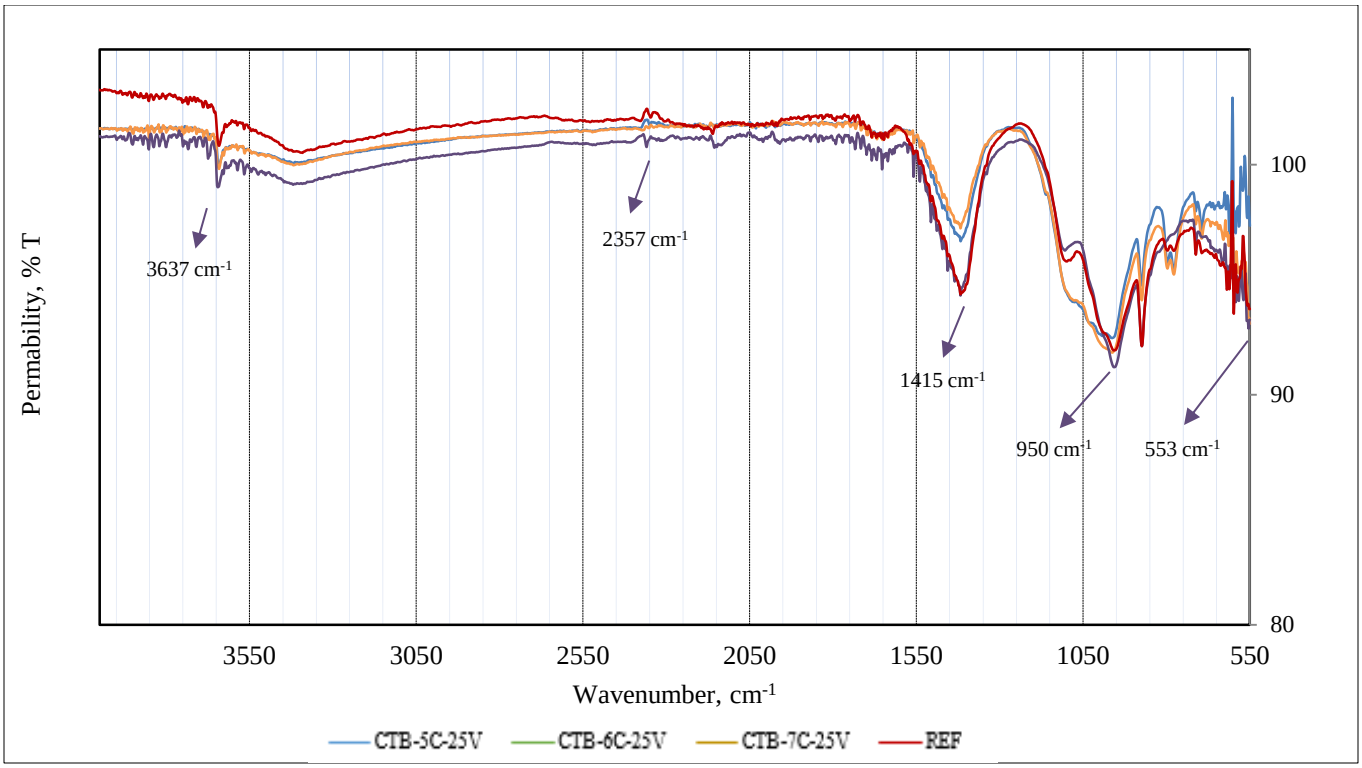

Figure 52. FT-IR results graph for the CTB-35V and REF concrete series

FT-IR results of the CTB-35V series

Figure 52 presents the FT-IR analysis results for four different samples from the CTB-35V series and the REF sample. Figure 52 shows the trend graph containing the FT-IR analyses of the CTB-35V and REF samples. This graph displays multiple peak points similar to those in Figure 50. The values for all series are quite similar to each other. The first peak for the CTB-35V and REF series is within the range of 3700 cm^{-1} and 3500 cm^{-1}. This range indicates the vibrations of OH groups or the presence of hydrated silicates (C-S-H). Upon examining the samples presented in the graph, these wavelengths demonstrate free OH groups or OH groups weakly bound by hydrogen bonds. Similar to Figure 50, the formed peaks determine the amount of free water in the cement during the hydration process. In the first peak, the sample CTB-7C-35V, with the highest wave amplitude, was identified with a wavenumber of 3637 cm^{-1}. In the second band area, peaks are observed at wavenumbers of 2400 cm^{-1} and 2000 cm^{-1}. These peak data are associated with CO2 absorption. The higher wavenumber and depth in the first two peaks were observed in the CTB-7C-35V (2357 cm^{-1}) sample. The peaks observed in the third region indicate the presence of water molecules during the cement hydration process. The highest depth in this region was reached by the REF (1409 cm^{-1}) and CTB-7C-35V (1415 cm^{-1}) samples. The third peaks indicate H-O-H bending vibrations. At the fourth peak and vibration point, unlike the graph seen in Figure 50, the deepest wave peak value was reached by the CTB-7C-35V sample with a wavenumber of 950 cm-1. This peak indicates Si-O stretching vibrations. It is observed that silicate hydrates (C-S-H) present in the cement are prominent at this wave amplitude. In the final peaks observed at the end of the graph, vibrations of compounds such as calcium silicates and aluminates are seen. The presence of minerals that constitute the main components of the cement is observed in these peak points. In the fifth peak of the CTB-7C-35V sample, it is understood that the region with the most intense presence of these minerals is at a wavenumber of 553 cm-1.

FT-IR results of the CTB-45V series

Figure 53 presents the FT-IR analysis results for four different samples from the CTB-45V series and the REF sample. Figure 53 shows the trend graph containing the FT-IR spectra of the CTB-45V and REF series. All examination and acceptance conditions are the same as those for the CTB-25V and CTB-35V series. The FT-IR values of all the series subjected to electrothermal curing,

along with the REF sample, formed very similar curves. In the graph shown in Figure 53, the deepest wave amplitude at the first peak (3637 cm^{-1}) was reached by the CTB-5C-45V sample. At the first peak, very close data in terms of wavelength were obtained for the other CTB-45V samples. This region shows the vibrations of the OH group. In this peak, it is possible to detect the bonding nature of the OH groups in the crystal structure and the presence of water. At the second peak point (2357 cm^{-1}), the absorption of carbonates and CO2 in the cement is observed. These peak points become more pronounced, especially when CO2 from the atmosphere adsorbs onto the cement or carbonates accumulate on the cement surface. At the third peak point (1409 cm^{-1}), the presence of water and bending vibrations are observed. Although the wavelengths and wavenumbers in this region are quite similar, the wave amplitude of the CTB-5C-45V sample is deeper compared to the other samples. The wavenumber of the CTB-5C-45V sample was found to be 1409 cm^{-1}. At the fourth peak point, the CTB-5C-45V sample again exhibited a deeper wave amplitude compared to the other samples. The wavenumber of the CTB-5C-45V sample was identified as 960 cm^{-1}. The peaks formed here indicate Si-O stretching vibrations. In the final section, the deepest wave amplitude was reached by the REF sample. The wavenumber of the REF sample was found to be 597 cm^{-1}. At this peak value, Al-O bonds are observed.

FT-IR results comparing the CTB-5C and REF series

Figure 54 presents the FT-IR analysis results for four different samples from the CTB-5C series and the REF sample. Figure 54 shows the FT-IR spectroscopy results for the samples cured with resistors placed at 5 cm intervals and the reference sample. In light of these analyses, the spectroscopy results for all CTB series and the REF sample are similar. Examination of the concrete series data reveals that shifts in peak positions and changes in peak intensities have affected the variations in hydration products. The largest peaks in all series were observed in the range of 1550 cm-1 to 800 cm-1. In the range of 4000 cm-1 to 3000 cm-1, a significant difference in permeability was noted compared to the samples cured with internal resistance. This difference was attributed to the rapid increase in hydration heat during setting in samples cured with internal resistance. The greatest absorption difference occurred at the third peak between the CTB-5C-25V and CTB-5C-35V samples. This difference at this point can be attributed to H-O-H bending vibrations. At the final peak, Al-O bond vibration peaks were observed (De and Pereira Gomes, 2005).

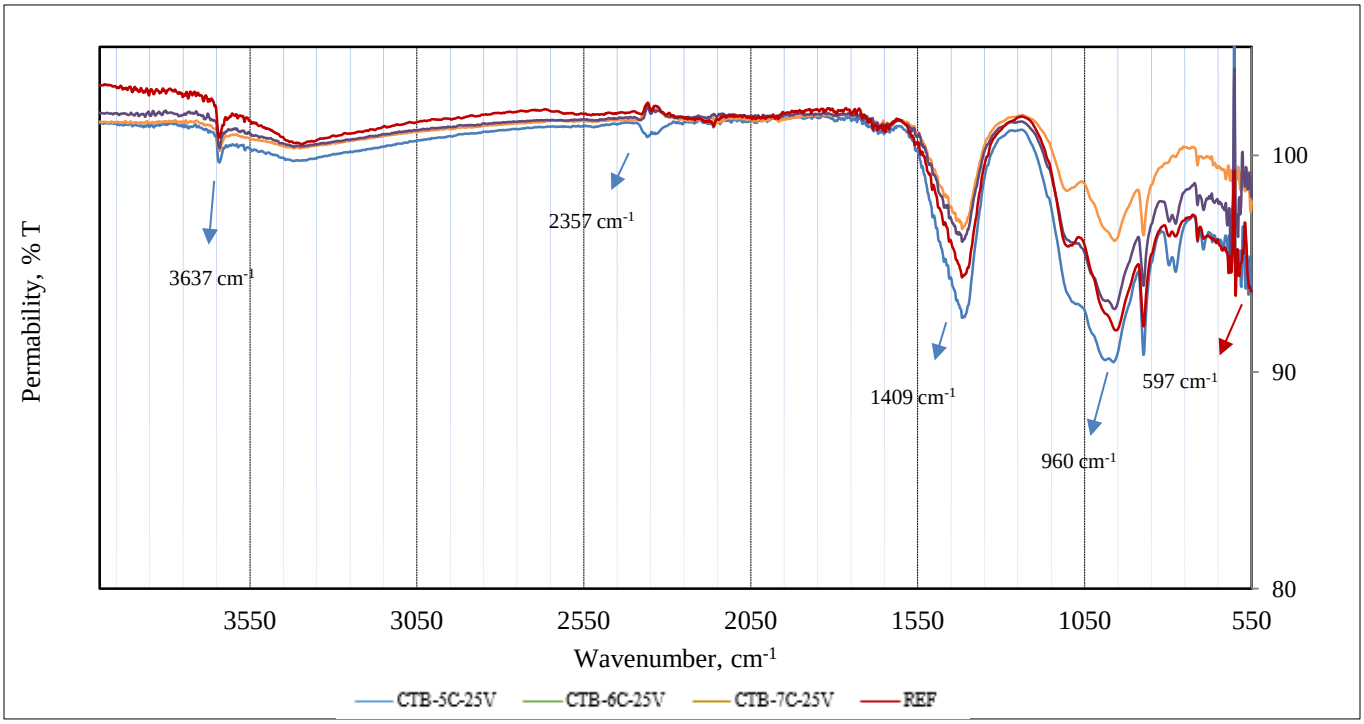

Figure 53. FT-IR results graph for the CTB-45V and REF concrete series

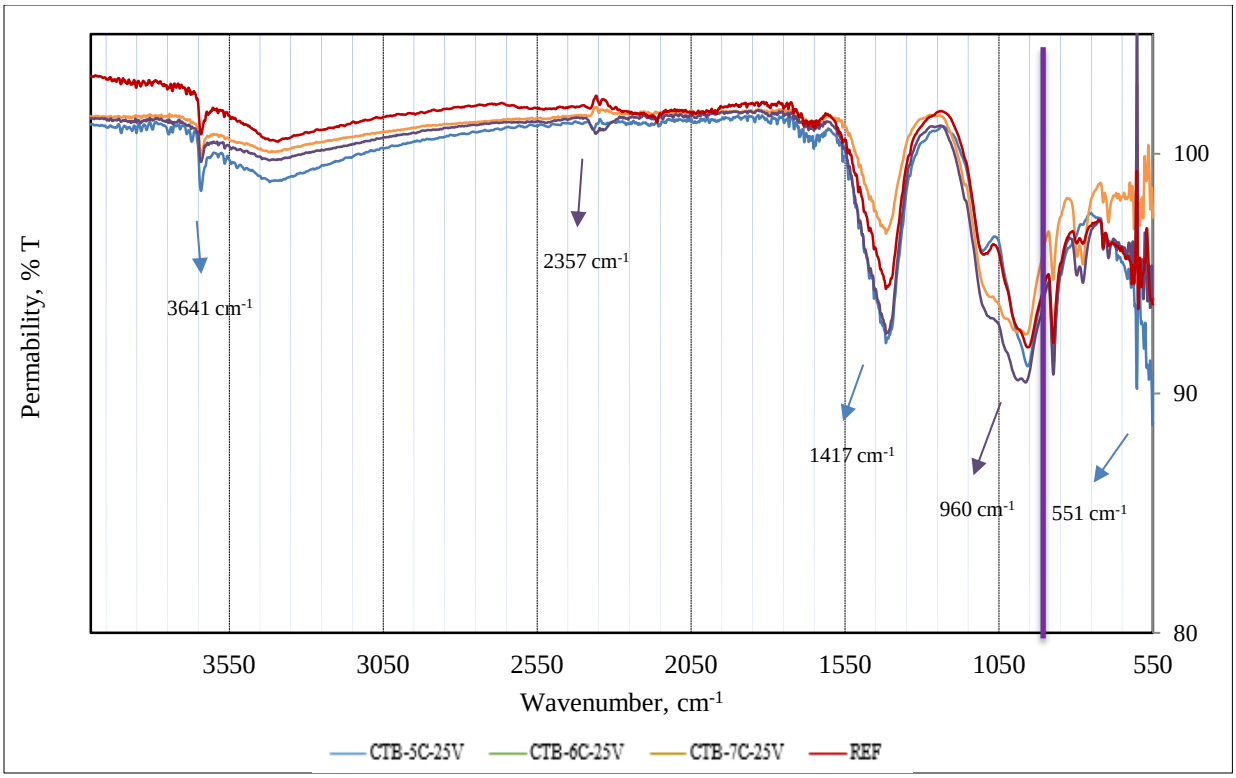

Figure 54. FT-IR results graph for the CTB-5C and REF concrete series

CONCLUSIONS

In situ casting concrete applications require that concrete gains early strength and meets the desired properties quickly, which is crucial for production speed. With advancements in technology and increased laboratory facilities, experimental methods have diversified. Increasing the internal temperature of concrete by embedding electrical resistors and producing hydration products more quickly and with better quality is essential. This study aimed to enhance the engineering properties of CTB samples using the internal resistance curing method. Resistors were placed at 5, 6, and 7 cm intervals in 50×50×4 cm concrete molds, with 25, 35, and 45 volts applied, and the samples were covered with stretch film to prevent moisture loss. The surface temperature, setting times, mechanical, and microstructural properties were examined by comparing with a reference sample.

- According to unit volume weight test results, a decrease in unit volume weight was observed in all series except for two series (CTB-5C-35V and CTB-6C-35V) as they aged. The unit volume weights of samples cured using the internal resistance method were lower compared to the reference sample. The lowest unit volume weight was observed in CTB-25V samples. Concrete series that achieved high unit volume weights at early ages experienced a decline in later ages. It was determined that the closure of the concrete molds to prevent air exposure was the reason for high unit volume weights at early ages.
- According to ultrasound transmission velocity data, the ultrasound transmission velocity of concrete is inversely proportional to the applied voltage. The ultrasound transmission velocity values for CTB-45V series were lower compared to other samples. On days 7, 14, and 28, the ultrasound transmission velocity values of the reference sample were higher than those of the samples cured with internal resistance. On the 14th day, the closest values to the reference sample were found in CTB-7C-35V and CTB-5C-35V samples, which were 1% lower. On the 28th day, the value of CTB-5C-35V sample approached that of the reference sample, with a difference of 0.5%. CTB-5C-35V showed the best results after the reference sample. Samples exposed to 45 volts created a porous and void structure due to high temperatures, which reduced concrete quality.
- According to bending strength test results, an increase in strength was observed in all concrete series as they aged. The reference sample showed a 17.1% increase between days 7 and 28. In CTB-25V series, these increases were 22%, 21%, and 19%; in CTB-35V series, 20%, 12%, and 30%; and in CTB-45V series, 19%, 24%, and 19%. The CTB-35V series provided the best results.

On day 28, the CTB-7C-35V sample achieved a bending strength that was 13% higher than the reference sample. This experiment demonstrated that concrete samples with higher bending strength can be obtained by applying 35 volts using the internal resistance method.

- According to compressive strength results, although the reference sample did not have high compressive strength at early ages, it was observed to be higher at later ages. The lowest values at 7 days were found in CTB-5C-25V (34.93 MPa) and the reference sample (35.67 MPa). The highest strength was found in CTB-6C-45V (39.73 MPa) series. Samples that showed high values at early ages fell behind due to the slower rate of strength increase at later ages. The reference sample, while having low compressive strength at early ages, reached 17% higher strength at later ages. The experiment showed that the effect of temperature is positive at early ages but negative at later ages.
- Thermal measurement results highlighted the importance of internal and surface temperatures of concrete during the setting process. The positive effects of curing with heat on mechanical strengths such as bending strength and early-age compressive strength were proven. The CTB-35V series generally provided the best results, while the 25-volt applied series showed the negative effects of low temperatures. It is known that high temperatures have both positive and negative effects on concrete's mechanical properties. The highest compressive strength at early ages was observed in CTB-45V series, but this series achieved the lowest values in ultrasound transmission velocity tests. This situation is consistent with literature indicating that high temperatures disrupt the microstructure of concrete.
- According to SEM analysis images, glass fiber reinforcement helped prevent vertical cracks, maintaining the composition of the concrete and improving mechanical strength. The large and numerous capillary voids in CTB-5C-25V sample led to low unit volume weight. In the CTB-5C-35V sample, the homogeneous distribution of the microstructure and the presence of minimal cracks and voids resulted in higher mechanical properties compared to other voltage-applied samples. In the CTB-5C-45V sample, deficiencies in hydration products, capillary voids, unhydrated cement grains, and cracks were detected due to high temperatures and evaporation, leading to low bending strength results.

Experimental results showed that the mechanical properties of the CTB-35V series are very close to or in some cases higher than the reference sample. In contrast, the CTB-25V and CTB-45V series exhibited lower values compared to the reference sample. These findings indicate that a 35-volt electrical current yields the best results in the internal resistance curing method.

When voltage is applied to concrete samples and the internal temperature of the concrete increases, the air and water in the cement rapidly expand and turn into gas. This creates micro voids in the sample and reduces the development of C-S-H. This laboratory study shows that curing with internal resistance limits the increase in strength. However, when concrete casting is needed at low temperatures, it is anticipated that desired strength increases can be achieved with the internal resistance curing method.

In addition to these experimental studies, investigating the durability properties of concrete cured with internal resistance is recommended. It is believed that this curing method will contribute to a more comprehensive understanding of its effects on glass fiber-reinforced concrete.

DECLARATIONS

Corresponding author

Correspondence and requests for materials should be addressed to Sıtkı Koc; E-mail: sitkikoc@outlook.com; ORCID: 0000-0003-1664-4938

Data availability

The datasets used and/or analysed during the current study available from the corresponding author on reasonable request.

Author's contribution

S.Koc, S.Subası, M.Maraslı and V.Ozdal contribute to the research, data analysis, and manuscript writing. S. Koc contributed to the conceptual design, formal analysis, methodology, software, research, original draft writing, visualization, review, and editing; S.Subası was responsible for project management, supervision, methodology, data curation, validation, software, and review; M.Maraşlı participated in supervision, visualization, resources, review, and editing; V.Özdal was involved in statistics and editing, review, resources, and analysis phases.

Acknowledgements

The authors thank Fibrobeton Yapı Elemanları San. ve İnşaat A.Ş for providing the resources in this research.

Consent to publish

Not applicable.

Competing interests

The authors declare no competing interests in this research and publication.

REFERENCES

Ali, A. M., Arslan, M. H., & Altın, M. (2019). Cam Lif Takviyeli Betonun Yangın Dayanımlarının Çeşitli Parametreler Açısından İrdelenmesi [Investigation of fire resistance of glass fiber reinforced concrete in terms of various parameters]. Doğal Afetler ve Çevre Dergisi, 5(2), 198-213. Available at: https://doi.org/10.21324/DACD.458094.

Backe, K.R., Lile, O.B. and Lyomov, S.K. (2001). Characterizing Curing Cement Slurries by Electrical Conductivity. SPE Drilling & Completion, 16(04), pp. 201–207. Available at: https://doi.org/10.2118/74694-PA.

Canbaz, M., Akçay, M. and Ergin, S. (2018). Elektriksel Direnç İle Istıma Yoluyla Uygulanan Kürün Beton Özelliklerine Etkisi. Uludağ Üniversitesi Mühendislik Fakültesi Dergisi, 23(1), pp. 431–440. Available at: https://doi.org/10.17482/UUMFD.419244.

Cong, J.-D., Liu, L. and Gou, K. (2016). The Study of Pre-control Temperature about the Concrete Curing Temperature with the Heating Cable.

De, F. and Pereira Gomes, E. (2005). Universidade Estadual De Campinas Viabilidade De Mudanças Tecnológicas Na Irrigação Da Tomaticultura [State University of Campinas Feasibility of Technological Changes in Tomato Irrigation]. Google Scholar

Deniz, E. (2011). Kür Şeklinin Yüksek Performanslı Betonların Mekanik Özelliklerine Etkisi [Effect of Curing Method on Mechanical Properties of High Performance Concretes], Dokuz Eylül Üniversitesi, Fen Bilimleri Enstitüsü, İnşaat Mühendisliği Bölümü, Yapı Malzemesi Anabilim Dalı, Yüksek Lisans Tezi, İzmir.

Doğan, F., Dehghanpour, H., Subaşı, S., & Maraşlı, M. (2022). Characterization of Carbon Fiber Reinforced Conductive Mortars Filled with Recycled Ferrochrome Slag Aggregates. Journal of Sustainable Construction Materials and Technologies, 7(3), 145-157. https://doi.org/10.47481/JSCMT.1157026.

Doğan, F., Dehghanpour, H., Subaşı, S., & Maraşlı, M. (2023). Experimental Investigation of Engineering Properties of Silica Sand Filled Mortars Containing High Doses of SWCNT. Gazi University Journal of Science Part C: Design and Technology, 11(1), 236-251. Available at: https://doi.org/10.29109/gujsc.1158688.

El-Dieb, A. S., El-Maaddawy, T. A., & Mahmoud, A. A. (2012). Water-Soluble Polymers as Self-Curing Agents in Cement Mixes. Advances in Cement Research, 24(5), 291-299. Available at: https://doi.org/10.1680/ADCR.11.00030.

Kjellsen, K.O. (1996). Heat Curing and Post-Heat Curing Regimes of High-Performance Concrete: Influence on Microstructure and C-S-H Composition. Cement and Concrete Research, 26(2), 295–307. Available at: https://doi.org/10.1016/0008-8846(95)00202-2.

Topçu, İ.B., Toprak, U. and Akdağ, D. (2008). Mikrodalga Kür Yöntemi ile Beton Dayanımın Erken Belirlenmesi [Early Determination of Concrete Strength by Microwave Curing Method]. Teknik Dergi, 19(94), 4539-4544. Google Scholar

Levita, G., Marchetti, A., Gallone, G., Princigallo, A., & Guerrini, G. L. (2000). Electrical properties of fluidified Portland cement mixes in the early stage of hydration. Cement and concrete research, 30(6), 923-930. Available at: https://doi.org/10.1016/S0008-8846(00)00282-9.

Lothenbach, B., Winnefeld, F., Alder, C., Wieland, E., & Lunk, P. (2007). Effect of Temperature on the Pore Solution, Microstructure and Hydration Products of Portland Cement Pastes. Cement and Concrete Research, 37(4), 483-491. Available at: https://doi.org/10.1016/J.CEMCONRES.2006.11.016.

Marasli, M., Guntep, S., Ozdal, V., Kohen, B., Dehgan, H., & Subasi, S. (2023). Development of Maturity Measurement Method and Device in Glass Fiber Reinforced Concrete (GRC). Available at: https://www.researchgate.net/publication/372413234.

Maraşlı M. (2019). Cam Lifi Takviyeli Betonlarda Olgunluk İndeksi Yöntemi İle Eğilme ve Basınç Dayanımlarının Tahmin Modelinin Geliştirilmesi [Development of a Model for Estimating Flexural and Compressive Strengths of Glass Fiber Reinforced Concretes Using Maturity Index Method], Yüksek Lisans Tezi [Master's Thesis], T.C. Düzce Üniversitesi Fen Bilimleri Enstitüsü, Kompozit Malzeme Teknolojileri Anabilim Dalı. Düzce. Google Scholar

Mathews, M. E., Kiran, T., Naidu, V. C. H., Jeyakumar, G., & Anand, N. (2021). Effect of high-temperature on the mechanical and durability behaviour of concrete. Materials Today: Proceedings, 42, 718-725. Available at: https://doi.org/10.1016/J.MATPR.2020.11.153.

Nazmul, R. T., Sainsbury, B. A., Al-Deen, S., Garcez, E. O., & Ashraf, M. (2023). An Experimental Evaluation of Hemp as an Internal Curing Agent in Concrete Materials. Materials, 16(11), 3993. Available at: https://doi.org/10.3390/MA16113993.

Nie, S., Hu, S., Wang, F., Yuan, P., Zhu, Y., Ye, J., & Liu, Y. (2016). Internal curing–a suitable method for improving the performance of heat-cured concrete. Construction and Building Materials, 122, 294-301. Available at: https://doi.org/10.1016/J.CONBUILDMAT.2016.05.159.

Nie, S., Zhang, W., Hu, S., Liu, Z., & Wang, F. (2018). Improving the fluid transport properties of heat-cured

concrete by internal curing. Construction and Building Materials, 168, 522-531. Available at: https://doi.org/10.1016/J.CONBUILDMAT.2018.02.068.

Pavlenko, S.I. (1994). Structure formation of slag ash concrete on the basis of high-calcium fly ash and silica fume', Materials and Structures, 27(7), pp. 401–407. Available at: https://doi.org/10.1007/BF02473444/METRICS.

Bentz, P. and Paul, E. (2006). Curing, Hydration, and Microstructure of Cement Paste. Available at: https://www.researchgate.net/publication/234155165_Curing_Hydration_and_Microstructure_of_Cement_Paste.

Puertas, F., Fernández-Jiménez, A. and Blanco-Varela, M.T. (2004). Pore solution in alkali-activated slag cement pastes. Relation to the composition and structure of calcium silicate hydrate', Cement and Concrete Research, 34(1), pp. 139–148. Available at: https://doi.org/10.1016/S0008-8846(03)00254-0.

Şahin, Y.İ. and Koçak, Y. (2022). Yüksek Fırın Cürufu İkameli Çimentoların Yapısal ve Mekanik Özelliklerinin Araştırılması', Düzce Üniversitesi Bilim ve Teknoloji Dergisi, 10(2), pp. 802–814. Available at: https://doi.org/10.29130/dubited.986896.

Sallı Bideci, Ö., Saka, R.C. and Bideci, A. (2017). Physical Characteristics of Rubberized Concrete Including Granulated Waste Tire Aggregate', Journal of Polytechnic, pp. 777–786. Available at: https://doi.org/10.2339/politeknik.368985.

Saran, A. et al. (2007). Certified Organization. International Journal of Innovative Research in Science, Engineering and Technology (An ISO, 3297).

Subasi, S., Dehghanpour, H. and Marasli, M. (2022). Production and Characterization of GRC-SWCNT Composites for Shell Elements. Medziagotyra, 28(4), 423–433. Available at: https://doi.org/10.5755/j02.ms.29008.

Türk Standartları Enstitüsü (2002). Beton - Sertleşmiş beton deneyleri - Bölüm 5: Deney numunelerinin eğilme dayanımının tayini [Concrete - Testing hardened concrete - Part 5: Determination of flexural strength of test specimens]. TS EN, 12390-5. Google Scholar

Uygunoğlu, T. and Hocaoğlu, İ. (2018). Effect of Electrical Curing Application on Setting Time of Concrete With Different Stress Intensity. Construction and Building Materials, 162, 298–305. Available at: https://doi.org/10.1016/j.conbuildmat.2017.12.036.

Whittington, H. W., McCarter, J., & Forde, M. C. (1981). The Conduction of Electricity through Concrete. Magazine of Concrete Research, 33(114), 48-60. Available at: https://doi.org/10.1680/MACR.1981.33.114.48.

Yıldırım, K., Sümer, M., & Yıldırım, Y. F. (2018). The İnvestigation of Metakaolin Effect on Concrete and Mortars Made with Agregates İncluding Reactive Silica. Mesleki Bilimler Dergisi (MBD), 7(2), 47-57. Available at: https://dergipark.org.tr/en/pub/mbd/issue/40281/441975 (Accessed: 14 July 2024).

Yoo, D.Y., Kim, S. and Kim, M.J. (2018). Comparative Shrinkage Behavior Of Ultra-High-Performance Fiber-Reinforced Concrete Under Ambient And Heat Curing Conditions. Construction and Building Materials, 162: 406–419. Available at: https://doi.org/10.1016/J.CONBUILDMAT.2017.12.029.